TWISTED DWARF1 mediates the action of auxin transport inhibitors on actin cytoskeleton dynamics

Jinsheng Zhu[1,19], Aurelien Bailly[1,2], Marta Zwiewka[3], Valpuri Sovero[2], Martin Di Donato[1], Pei Ge[1,15], Jacqueline Oehri[1,4], Bibek Aryal[1], Pengchao Hao[1], Miriam Linnert[6,18], Noelia Inés Burgardt[6,7], Christian Lücke[6], Matthias Weiwad[6,17], Max Michel[8], Oliver H. Weiergräber[8], Stephan Pollmann[9], Elisa Azzarello[10], Stefano Mancuso[10], Noel Ferro[11], Yoichiro Fukao[5,16], Céline Hoffmann[13], Roland Wedlich-Söldner[12], Jiří Friml[14], Clément Thomas[13] and Markus Geisler[1,2,20]

[1] University of Fribourg, Department of Biology, Fribourg, Switzerland
[2] University of Zurich, Department of Plant and Microbial Biology, CH-8008 Zurich, Switzerland
[3] Mendel Centre for Plant Genomics and Proteomics, Central European Institute of Technology (CEITEC), Masaryk University (MU), Kamenice 5, Brno, Czech Republic.
[4] Institute of Evolutionary Biology and Environmental Studies, University of Zurich, Zurich, Switzerland
[5] Plant Global Educational Project, Graduate School of Biological Sciences, Nara Institute of Science and Technology, Ikoma, Japan
[6] Max Planck Research Unit for Enzymology of Protein Folding, Halle (Saale), Germany
[7] Institute of Biochemistry and Biophysics (IQUIFIB), School of Pharmacy and Biochemistry, University of Buenos Aires, Buenos Aires, Argentina.
[8] Institute of Complex Systems, ICS-6: Structural Biochemistry, Jülich, Germany.
[9] Centro de Biotecnología y Genómica de Plantas, Campus de Montegancedo, Madrid, Spain.
[10] LINV- DIPSAA - Università di Firenze, 50019 Sesto F. no (FI), Italy.
[11] University of Bonn, Mulliken Center for Theoretical Chemistry, Institute for Physical and Theoretical Chemistry, Bonn, Germany
[12] Institute of Cell Dynamics and Imaging, University of Münster, D-48149 Münster, Germany
[13] Cytoskeleton & Cancer Progression, Laboratory of Experimental Cancer Research, Department of Oncology. Luxembourg Institute of Health, 84 Val Fleuri, L-1526 Luxembourg, Luxembourg
[14] Institute of Science and Technology (IST) Austria, Klosterneuburg, Austria.
[15] present address: Station Biologique de Roscoff, CNRS-UPMC, Place Georges Tessier, CS 90074, 29688 Roscoff, France.
[16] present address: Department of Bioinfomatics, Ritsumeikan University, Shiga, Japan.
[17] Martin-Luther-University Halle-Wittenberg, Institute of Biochemistry and Biotechnology, Department of Enzymology, Halle, Germany
[18] present address: Fraunhofer Institute for Cell Therapy and Immunology IZI, Department of Drug Design and Target Validation, Halle, Germany
[19] present address: Structural Plant Biology Laboratory, Department of Botany and Plant Biology, 1211 Geneva, Switzerland
[20] to whom correspondence should be addressed: markus.geisler@ unifr.ch

Running title: TWD1 regulates actin cytoskeleton dynamics

1

Synopsis: TWISTED DWARF1 determines downstream locations of auxin efflux transporters by adjusting actin cytoskeleton dynamics and mediates NPA action on these in an action that is evolutionary conserved.

ABSTRACT

Plant growth and architecture is regulated by the polar distribution of the hormone auxin. Polarity and flexibility of this process is provided by constant cycling of auxin transporter vesicles along actin filaments, coordinated by a positive auxin-actin feedback loop. Both polar auxin transport and vesicle cycling are inhibited by synthetic auxin transport inhibitors, such as 1-*N*-naphthylphthalamic acid (NPA), counteracting the effect of auxin; however, underlying targets and mechanisms are unclear. Using NMR, we map the NPA binding surface on the Arabidopsis ABCB chaperone, TWISTED DWARF1 (TWD1). We identify ACTIN7 as a relevant - although likely indirect - TWD1 interactor, show TWD1-dependent regulation of actin filament organization and dynamics, and that TWD1 is required for NPA-mediated actin cytoskeleton remodeling. The TWD1-ACTIN7 axis controls plasma membrane presence of efflux transporters and as a consequence *act7* and *twd1* share developmental and physiological phenotypes indicative of defects in auxin transport. These can be phenocopied by NPA treatment or by chemical actin (de)stabilization. We provide evidence that TWD1 determines downstream locations of auxin efflux transporters by adjusting AF de-bundling and dynamizing processes and mediating NPA action on the latter. This function appears to be evolutionary conserved since TWD1 expression in budding yeast alters actin polarization and cell polarity and provides NPA sensitivity.

INTRODUCTION

In land plants, virtually all developmental processes are dependent on the formation of local maxima and minima of the plant hormone auxin (Vanneste and Friml, 2009; Kania et al., 2014). These auxin gradients are created by the cell-to-cell transport of auxin, designated as polar auxin transport (PAT; Vanneste and Friml, 2009). Due to the chemical properties of the main relevant auxin, indolyl-acetic acid (IAA), PAT is thought to be established and regulated mainly by the action of precisely tuned plasma membrane auxin exporters of the PIN-FORMED and ABCB/PGP families (Geisler and Murphy, 2006; Vanneste and Friml, 2009; Geisler et al., 2014). Both PINs and ABCBs are thought to constantly cycle between the plasma membrane (PM) and endosomal compartments associated with the trans-Golgi network, which requires the brefeldin A (BFA)-sensitive

ARF-GEF (Exchange factors for ARF GTPases), GNOM (Geldner et al., 2001; Cho et al., 2007; Kleine-Vehn and Friml, 2008; Titapiwatanakun et al., 2009; Wang et al., 2013). In contrast to the mainly polarly expressed PINs, widely non-polar ABCBs are less dynamic in PM trafficking (Titapiwatanakun et al., 2009; Cho et al., 2012). However, dynamics of both auxin exporter subclasses are dependent on actin filament (AF) organization providing tracks for secretory vesicle delivery (Geldner et al., 2001; Kleine-Vehn et al., 2006; Dhonukshe et al., 2008).

The plasma membrane presence of ABCBs is dependent on the FKBP42 (FK506-binding protein) TWISTED DWARF1 (TWD1) acting as a chaperone of ER to PM provision of ABCB1, ABCB4 and ABCB19 (Wu et al., 2010; Wang et al., 2013; Zhu and Geisler, 2015; Geisler et al., 2016). Therefore these ABCBs, but not PIN1 or PIN2, are delocalized and degraded in *twd1* (Bouchard et al., 2006; Wu et al., 2010; Wang et al., 2013; Bailly et al., 2014). As a result, polar auxin transport is drastically reduced in *abcb1 abcb19* and *twd1*, leading to widely overlapping phenotypes, including dwarfism, disoriented growth and helical rotation (twisting) of epidermal layers (Geisler et al., 2003; Wu et al., 2010; Wang et al., 2013). Epidermal twisting in *twd1/fkbp42* is in contrast to mutations of tubulin subunits, such as the *O. sativa* (rice) mutant *twisted dwarf1* (*td1*; Szymanski et al., 2015), non-handed. The chaperone function of TWD1/FKBP42 is in functional analogy with the closest mammalian ortholog, FKBP38, shown to chaperone ABCC7/CFTR to the PM (Banasavadi-Siddegowda et al., 2011), but underlying mechanisms are not clear.

Our knowledge on the mechanisms of PAT and auxin transporter trafficking has been expanded by the usage of synthetic auxin transport inhibitors, such as NPA, a non-competitive auxin efflux inhibitor (Cox and Muday, 1994; Butler et al., 1998). At low concentrations (1-5 μM), NPA efficiently inhibits the basal polar auxin flow required for plant development. Moreover, growth of Arabidopsis on NPA (or its functional analog, BUM (Kim et al., 2010)) induces pin-formed inflorescences phenocopying the loss-of-function mutant of the auxin exporter, *PIN-FORMED1* (*PIN1*). However, definitive data demonstrating NPA binding and direct transport inhibition for PIN proteins are lacking ((Petrasek et al., 2006; Rojas-Pierce et al., 2007; Kim et al., 2010); Figure 1). Therefore, it seems obvious that NPA acts on PIN-dependent auxin transport (Petrasek et al., 2003; Petrasek et al., 2006); however, by an unknown mechanism involving additional but so far not characterized regulators.

At high (>50 μM) concentrations, NPA seems to block PAT by affecting trafficking components (Geldner et al., 2001; Gil et al., 2001; Peer et al., 2009). One mode of NPA action likely affects the actin cytoskeleton, as NPA alters AF organization, especially the

3

extent of actin bundling. By F-actin imaging, it was demonstrated that long-term treatment with NPA (10 μM, 48h) decreased filamentous actin and generated punctuated structures in root epidermal cells (Rahman et al., 2007; Zhu and Geisler, 2015). The opposite effects of auxins and auxin transport inhibitors on actin bundling raised the question of whether auxin transport inhibitors act indirectly via local accumulation of auxin concentrations (Rahman et al., 2007). This possibility, however, is less likely as auxin transport inhibitors induce actin bundling in non-plant cells also (Dhonukshe et al., 2008).

Results of *in vitro* experiments have indicated that auxin transport inhibitors do not act on AF bundling directly (Dhonukshe et al., 2008) but rather require a not-yet characterized NPA-binding protein (NBP) mediating the remodeling action of NPA on the actin cytoskeleton (Zhu and Geisler, 2015). Plant cells contain NPA-binding proteins, although their exact number, identity and modes of action remain surprisingly unclear (Luschnig, 2002; Zhu and Geisler, 2015). Based on biochemical *in vitro* assays, NBPs were reported to be PM-associated and NPA-binding activity was localized to the cytoplasmic face of the membrane (Cox and Muday, 1994). Moreover, a peripheral NPA-binding protein was suggested to be associated with the cytoskeleton (Cox and Muday, 1994; Dixon et al., 1996; Butler et al., 1998). ABCB-type auxin transporters and TWD1 were originally identified by NPA-chromatography and subsequently verified as NPA targets (Murphy et al., 2002; Geisler et al., 2003; Rojas-Pierce et al., 2007; Nagashima et al., 2008; Kim et al., 2010). Using radiochemistry, NPA was shown to bind to the putative FKBD (FK506-binding protein domain) of TWD1 that also serves as a binding surface for ABCB-TWD1 interaction (Granzin et al., 2006; Bailly et al., 2008). Interestingly, micromolar concentrations of NPA disrupt ABCB1-TWD1 interaction, suggesting that NPA binds at the ABCB-TWD1 interface (Bailly et al., 2008).

The current picture that emerges is that auxin regulates its own transport by fine-tuning (unbundling) the organization of AFs (Holweg et al., 2004; Paciorek et al., 2005; Zhu and Geisler, 2015). Auxin transport inhibitors would counteract this effect by promoting AF bundling and subsequent auxin exporter vesicle trafficking defects and thus altered PAT (Kleine-Vehn et al., 2006; Dhonukshe et al., 2008). However, the mechanism by which auxin transport inhibitors modulate actin cytoskeleton organization remains to be explored. Here we searched for a functional role for NPA-binding to the FKBP42, TWD1. Our data reveal that TWD1 regulates AF dynamizing and de-bundling processes, and confers the modulatory effect of NPA on actin cytoskeleton remodeling. We precisely map the NPA binding surface on TWD1, which binds at the same time the vegetative actin subunit ACTIN7. Loss of function of *ACT7* results in mislocation of auxin exporters of PIN and

ABCB subclasses and produces developmental phenotypes that are phenocopied pharmacologically by actin (de)stabilizing drugs or genetically by *TWD1* loss of function, respectively. These observations support a function for TWD1 in cytoskeleton-dependent auxin exporter trafficking in an action that seems to be evolutionary conserved and that is consistent with its previously suggested chaperone function (Wu et al., 2010; Wang et al., 2013; Zhu and Geisler, 2015).

RESULTS

The FK506-binding domain of TWD1 binds NPA with low affinity and *TWD1* loss of function results in reduced NPA sensitivities

To identify residues of the FK506-binding protein (FKBP) domain (FKBD) of TWD1 implicated in NPA binding (Bailly et al., 2008), we employed chemical shift perturbation (CSP) mapping based on the previously reported NMR resonance assignment of the TWD1 FKBD (Burgardt et al., 2012). Changes in the backbone amide signal positions of ^{15}N-labelled TWD1$^{1-180}$ in the absence and in presence of NPA were analyzed (Figure 1A; Supplemental Figure 1) and mapped onto the X-ray structure of the TWD1 FKBD (PDB 2F4E; Weiergraber et al., 2006). The most pronounced shifts were observed for residues K39, V40, D41, T78, K79, S81, Q82, H83, A122, L123, V124 and Y151, indicating that the NPA contact region is located outside of the putative PPIase (*cis-trans* peptidylprolyl isamerase) site of the FKBD at the convex face of the half β-barrel (Figure 1B). Quercetin, a putative auxin transport inhibitor shown not to bind to TWD1 (Bailly et al., 2008), revealed no major CSP shifts, thus indicating specificity of the binding for NPA.

To corroborate the NMR data and to better understand the supra-molecular NPA association with the FKBD structure, we employed *in silico* NPA docking on the entire TWD1 structure available (PDB 2IF4; Granzin et al., 2006) and on the FKBD (PDB 2F4E; Weiergraber et al., 2006) using PyMOL embedded the AutoDock Vina toolset (Seeliger and de Groot, 2010; Bailly et al., 2012). Rigid *in silico* NPA docking followed by flexible side-chain optimization verified the FKBD as major NPA target and the predicted binding region correlates well with the one showing CSP value changes (Supplemental Figure 2).

Further, we used quantum chemical modeling based on density functional theory including dispersion correction terms (DFT-D; Effendi et al., 2014) to optimize the binding geometry of the NPA interaction using the crystal structure of the TWD1 FKBD (PDB 2F4E; Weiergraber et al, 2006) as the basis. The statistical analyses of different components of the quantum chemical forces and the electron density distribution in the region of interaction pocket-NPA deformation suggest that Van der Waals forces (ΔE_{VdW}) are

primarily responsible for NPA binding to the TWD1 surface (Supplemental Figure 3), as has been recently proposed for other small molecule-protein interactions using thermodynamic data (Barratt et al., 2005). Further, they suggest that a direct contact is provided by amino acid residues Q82, K79, H125 and D41 (Figure 1C). Strikingly, both *in silico* techniques suggest a nearly identical pocket for NPA binding and identify widely overlapping putative NPA contact residues, which are in good agreement with the NMR data (Figure 1B-C; Supplemental Figure 2). Further, both tools revealed highly reduced internal binding energies (ΔE_{ave}(NPA) = -71.65 kJ/mol; $\Delta E_{(ave)}$(BA) = -31.35 kJ/mol) and AutoDock Vina top-ranked docking pose scores (NPA = -11 kcal/mol and BA = -4 kcal/mol for flexible side chains mode) for benzoic acid (BA) in comparison to NPA, respectively. The former is commonly used as a negative control in auxin research and both methods exclude BA binding to TWD1 (Supplemental Figure 2).

These *in vitro* and *in silico* data allowed us to design point mutations in the putative NPA binding surface with the goal of generating a version of TWD1 that is NPA insensitive. Four out of five FKBD mutations - TWD1^{K79I}, TWD1^{H125I}, TWD1^{P37L} and TWD^{K39I} - abolished NPA binding (Supplemental Figure 4), which based on chemical modeling, is mainly caused by loss of van der Waals forces (ΔE_{VdW}, Supplemental Figure 3) to the ligand, NPA. In TWD1^{P37L}, NPA binding seems to be affected additionally by massive protein deformation (ΔE_{Pdef}) resulting in positive $\Delta\Delta E$ and $\Delta\Delta E_{ave}$ based on constrained geometry optimization and full geometry optimization, respectively (Supplemental Figure 3). Interestingly, TWD1^{Q82A} revealed higher NPA binding but with lower specificity shown by benzoic acid binding assayed in parallel (Supplemental Figure 4). The latter finding is in agreement with lower calculated binding energies ($\Delta\Delta E_{ave}$ = -21.43 kJ/mol for the full geometry optimization) and the presence of very similar chemical forces in comparison to the WT protein according to the quantum chemical modeling (Supplemental Figure 3). TWD1 K79 was identified by NMR and both *in silico* dockings to be involved in NPA binding and TWD1^{K79I} exhibited reduced NPA binding (in line with reduced $\Delta\Delta E_{ave}$ = 6.92 kJ/mol for the constrained geometry optimization). TWD1^{K79I} was one of the most distant mutants in the multivariable analysis of the calculated chemical forces of the binding energies (Supplemental Figure 3) and retained its capacity to regulate ABCB1-mediated auxin transport (Supplemental Figure 4) and was therefore selected for further studies.

To test other auxin transport inhibitors for TWD1 binding, we employed surface plasmon resonance (SPR) analyses of recombinant *Arabidopsis* TWD1$^{1-339}$ protein cross-linked to sensor chips by thiol coupling. We chose this immobilization strategy over the classical amine coupling because K79 and K39 were part of the putative NPA binding surface, while

TWD1 contains four cysteine residues that are outside of this domain. NPA exhibited concentration-dependent SPR responses (Figure 1D), verifying previous binding studies using radiochemistry (Bailly et al., 2008; Kim et al., 2010). Kinetic binding constants were approximated using a 1:1 Langmuir fit model, although sensograms did not always strictly follow pseudo-first order kinetics, which was most obvious for TIBA (triiodobenzoic acid). However, K_D's obtained from both kinetic and equilibrium analyses ($K_{D(kin)}$ = 105 $\pm$ 12 μM, $K_{D(eq)}$ = 133 $\pm$ 20 μM; Table 1 and Supplemental Fig. 5) qualify the TWD1$^{1-339}$ protein as a low-affinity NPA binding protein *in vitro*, which is in agreement with small NMR shifts (Figure 1). Amine coupling of TWD1$^{1-339}$ enhanced higher-order kinetic behavior of interactions and thus required a 1:2 surface heterogenicity fit model resulting in K_D's for NPA of 135 and 910 μM (data not shown). This supports an inactivation of the binding surface in a portion of the immobilized TWD1 protein, most likely by K79 and K39 coupling.

The electronic binding energy ΔE and the average of the internal energies ΔE_{ave} for NPA calculated by quantum chemical modeling (ΔE = -92.56 kJ/mol, ΔE_{ave} = -71.65 kJ/mol) cannot be precisely converted into ΔG values. However, taking into account the dominating influence of Van der Waals interactions and therefore excluding the entropy as major binding driver, a direct transformation (see Methods for details) suggested a ΔG between -20.92 and -29.29 kJ/mol. This is in agreement with the experimental SPR data, as a K_D of 105 μM gives a theoretical ΔG of -22.614 kJ/mol (Table 1).

As expected, other auxin efflux inhibitors, like TIBA, and BUM (2-[4-(diethylamino)-2-hydroxybenzoyl benzoic acid; Kim et al., 2010) bound to TWD1 although with lower affinities (Table 1), while the unspecific diffusion control, benzoic acid, did not (Table 1; Supplemental Fig. 5), verifying experimentally the *in silico* data.

To complement these *in vitro* studies, we quantified specific NPA binding to microsomes prepared from *TWD1* and auxin exporter loss-of-function mutants. In agreement with low-affinity NPA binding to TWD1 and low expression of *TWD1*, we found slightly but significantly reduced NPA binding for *twd1* microsomes (Figure 1E). Reduced binding was also found for *abcb1* and *abcb19* material (Rojas-Pierce et al., 2007; Kim et al., 2010) but not for *pin1* and *pin2/eir1-4*, verifying the idea that direct NPA binding primarily affects the TWD1-ABCB complex (Petrasek et al., 2006; Rojas-Pierce et al., 2007; Kim et al., 2010).

In light of the above, we tested the *in planta* sensitivity of the *twd1* mutant towards NPA in auxin-regulated developmental processes (Bailly et al., 2008). Quantification of apical hook opening (see below), root gravitropism and hypocotyl elongation (Supplemental

Figures 6 and 7) revealed that *twd1* is widely NPA insensitive, while over-expression of HA-TWD1 in *twd1-3* complemented the NPA insensitivity of the mutant (Supplemental Figure 6).

TWISTED DWARF1 indirectly interacts with ACTIN7

To identify downstream targets of a low-affinity, NPA-mediated TWD1 action we employed a co-immunoprecipitation (co-IP) approach followed by MS/MS analyses similar to Henrichs et al. (2012) but using whole TWD1:TWD1-CFP roots as starting material. Three independent co-IP/MS analyses identified 51 common, putative TWD1 interacting proteins (Supplemental Table 1). These showed a remarkable enrichment of plasma membrane (PM) proteins with a few suggested molecular functions, such as transporter activity (20%), protein binding (23%) and GTPase activity (8%; Supplemental Figure 7). Interestingly, we preferentially pulled-down proteins (such as ABCB4, HSP90, ABCC1, ABCC2 and calmodulin) that either have already been shown to interact with TWD1 (Kamphausen et al., 2002; Geisler et al., 2003; Geisler et al., 2004; Wu et al., 2010; Wang et al., 2013) or to putatively function in protein trafficking (RAB GTPases, DYNAMIN-LIKE 3, CLATHRIN and ACTIN7). We selected ACTIN7 (ACT7; score: 278, number of sequences: 9, emPAI: 1.3) for further analyses based on the following: First, ACT7 and ACT8 were previously pulled-down with 35S:TAP1-TWD1 (Henrichs et al., 2012) and HA-TWD1 (not shown) but also with ABCB1:ABCB1-MYC (not shown), suggesting that ACT7 (and possibly also ACT8) is part of the TWD1-ABCB1 efflux complex. Second, *ACT7* is strongly expressed in young plant tissues and is induced by auxin, and *act7* alleles cause a reduction in root growth and increased root slanting and waving, resembling the *twd1* mutant phenotype (Kandasamy et al., 2009).

Identification of ACT7 as a TWD1 interactor does not necessarily imply direct physical interaction. To assess the ability of TWD1 to autonomously bind AFs and to map the potential actin-binding region, high-speed co-sedimentation assays were conducted with TWD1$^{1-180}$ (FKBD) and TWD1$^{1-339}$ and rabbit muscle actin in various conditions of calcium and pH (Papuga et al., 2010). As exemplified for FKBD (Supplemental Figure 9A), both the truncated and full-length proteins mostly remained in the supernatant fraction, and only a faint amount (< 5%) was detected in the pellet fraction together with AFs. Because a similar portion of TWD1$^{1-180}$ and TWD1$^{1-339}$ also sedimented in control experiments (*i.e.* without actin), we considered it as being unspecific. As an additional indication that TWD1 does not interact with AFs in a direct manner, it had no effect on the actin polymerization rate in pyrene-actin assays conducted in the absence or presence of NPA (Supplemental

8

291 Figure 9B).

292

TWISTED DWARF1 regulates actin cytoskeleton organization and dynamics and
293
294 **mediates the effect of NPA on actin filament turnover**

295 To gain insight into a putative functional link between TWD1 and the actin cytoskeleton, we
296 carefully examined actin filament organization in WT and *twd1-1* seedlings in which we
297 introduced the actin reporter GFP-fABD2 (Sheahan et al., 2004). Employing variable angle
298 epifluorescence microscopy (VAEM), we noticed that, as compared to WT hypocotyls,
299 *twd1-1* exhibited fewer thick and bright filamentous structures corresponding to actin
300 bundles (Figure 2). To confirm and extend these data, actin filament bundling (skewness)
301 and density (percent of occupancy) were quantified in the hypocotyl epidermal cells from
302 dark-grown seedlings following established protocols (Higaki et al., 2010). Average
303 skewness values of 2.84 ± 0.05 and 2.29 ± 0.06 were calculated for WT and *twd1-1*
304 hypocotyls, respectively (Figure 2B), confirming that loss of *TWD1* lowers the overall
305 cellular level of actin bundling. In addition, and most likely as a result from reduced actin
306 bundling, actin filament density was increased in *twd1-1* (Figure 2A,C). Interestingly, long-
307 term treatment with NPA (10 μM, 5 dag) induced prominent cytoskeletal changes in WT
308 hypocotyls with a 40% increase in actin bundling and 35% decrease in actin filament
309 density (Figure 2A-C), similar to what has been reported before for the auxin transport
310 inhibitors, PBA and TIBA (Dhonukshe et al., 2008). The absence of an effect of NPA on
311 actin stability in previous studies might be due to shorter treatments and/or a lower
312 microscopical resolution compared to our VAEM analyses (Petrasek et al., 2003;
313 Dhonukshe et al., 2008).

314 In striking contrast to WT, NPA had no significant effect on actin filament bundling and
315 density in *twd1-1* hypocotyls (Figure 2A-C), indicating that NPA-mediated actin bundling
316 requires TWD1. Interestingly, *act7-4* hypocotyls exhibited excessive bundling as compared
317 to WT. However, like in *twd1-1,* the extent of actin bundling was insensitive to NPA, further
318 supporting a functional TWD1-ACT7 interaction. The NPA resistance of *twd1-1* and *act7-4*
319 hypocotyls was confirmed using standard confocal microscopy analyses of identical GFP-
320 fABD2 lines (Supplemental Fig. 10 vs. Fig. 2) using described methods (Higaki et al.,
321 2010). We found that *twd1-1* and *act7-4* were insensitive to NPA in tested concentrations
322 up to 100 μM, while bundling reached already a saturation at 10 μM NPA in the hypocotyls
323 of WT and *twd1-1* hypocotyls complemented by TWD1:TWD1-CFP (Supplemental Fig.
324 11). The bundling defects caused by low μM NPA concentrations in WT hypocotyls might
325 at first view seem contradictory to the relatively high K_D value (~ 105 μM) that we obtained

9

by SPR analyses. However, it is likely that NPA accumulates within tissues and can locally reach high concentrations, especially after long-term treatments as those used in our culture conditions. Moreover, binding affinities generated *in vitro* might considerably differ from those *in planta*.

In addition to the static analyses above, we quantified several parameters of single actin filament dynamics (Staiger et al., 2009; Henty-Ridilla et al., 2013; Hoffmann et al., 2014b). In WT, cortical AFs exhibited typical dynamics including a relatively short lifetime (31 ± 7.4 s), and high elongation rate and severing frequency (2.9 ± 1.0 µm/s and 0.011 ± 0.004 breaks/µm/s, respectively; Table 2) that are in good agreement with previous data (Henty et al., 2011). In *twd1-1*, actin filament lifetime was significantly higher than in WT with an average of 45.1 ± 10.3 s. This increase in actin filament stability was consistent with a reduced de-polymerization rate and severing frequency (see Supplemental Movies 1-3). NPA treatment altered virtually all parameters of actin filament dynamics in WT hypocotyls. Consistent with the fact that NPA increases the overall level of actin bundling (Figure 2), it lowered actin filament dynamics as shown by an increase in actin filament lifetime and length and a decrease in actin filament severing (see Supplemental Movies 4-6). Most remarkably, and in agreement with the inability of NPA to promote actin bundling in *twd1-1* hypocotyls, none of the single actin filament dynamic parameters analyzed was affected by NPA treatment in *twd1-1* (Table 2).

Our data revealed that bundling frequencies of AFs were similar in WT and *twd1-1* hypocotyls (Table 2). By contrast, de-bundling frequency was much (nearly 4-times) higher in *twd1-1,* which seems to account for the reduced overall bundling level observed in *twd1-1* hypocotyls (Figure 2). Thus, it appears that TWD1 triggers a dual action on actin cytoskeleton organization and dynamics in hypocotyls: on one hand, it stimulates single AF dynamics, *e.g.* by increasing AF de-polymerization and severing, and on the other, it down-regulates the process of de-bundling. Surprisingly, NPA reduced actin bundling and de-bundling frequencies by about 50% in both WT and *twd1-1* hypocotyls (see Table 2). This unexpected result suggests that, in addition to its TWD1-dependent action on single AF dynamics, NPA may modulate the processes of actin bundling/de-bundling in a TWD1-independent manner. Consistent with the fact that actin bundling and de-bundling frequencies were similarly reduced by NPA, NPA treatment had no apparent effect on the overall actin bundling level and AF density in *twd1-1* (Figure 2B and C; Supplemental Fig. 10B and 11B).

ACT7 regulates expression and location of ABCB and PIN-type auxin exporters and

of TWD1

The known role of the actin cytoskeleton in auxin transporter cycling (Geldner et al., 2001; Kleine-Vehn et al., 2006; Dhonukshe et al., 2008) and delocalization of ABCBs in *twd1* (Wu et al., 2010; Wang et al., 2013) prompted us to investigate the locations of auxin transporters in *act7-4*. We found that expression of ABCB1-GFP and ABCB19-GFP and, most drastically, ABCB4-GFP was significantly down-regulated in *act7-4* and that all tested ABCBs were partially retained on intracellular structures (Figures 3-4). PIN1-GFP and PIN2-GFP were likewise found on similar structures and their polarity was reduced (Figures 3-4). However, in contrast to ABCBs, expression of PIN2 was less affected, while expression of PIN1 was even slightly up-regulated (Figure 3C). To our surprise TWD1-CFP was also partially delocalized from ER/PM locations in *act7-4* (Figure 3B), which is in line with the proposed chaperone function of TWD1 during ER to PM secretion of ABCBs (Wu et al., 2010; Wang et al., 2013). Moreover, TWD1 lost lateral PM polarity (Wang et al. 2013) in immunostained roots of *act7* single and double loss-of-function mutant material (Supplemental Figure 12). We noticed that both endosomal structures and transporter de-localizations in *act7-4* were often found in misshaped cells (Figures 3-4). A thorough investigation employing PIN2-GFP and propidium iodide staining of cell walls revealed that these defects indeed are found in misshaped cells but that they do not strictly correlate with cell wall defects (Figures 3-4). De-localizations for PIN1,2-GFP and ABCB4-GFP were also not caused by non-isogenic ecotype backgrounds (see Methods for details) as revealed by immunolocalization of PIN1,2 in *act7-4* and crossings between ABCB4-GFP and *act7-6* lines that are both in the Col-0 background (Supplemental Figure 13).

Short treatments with endocytic tracer FM4-64 (2 μM, 15 min) resulted in FM4-64 accumulation into internal (probably TGN or early endosomal) structures in *act7-4* and, more severely, in actin double mutants but not in *twd1* (Supplemental Figure 12A) suggesting a role for ACT7 in endosomal balance. An early endosomal/TGN marker, ARF1, showed a similarly defective distribution in *act7-4* and *act7-4 twd1-1* but not in *twd1-1*, verifying the endosomal identity of defective endomembranes (Supplemental Figure 12B). Lysotracker red (LTR) and long-term FM-4-64 (4 μM, 3 h) applications revealed additionally aberrant vacuolar morphologies (Supplemental Figure 12C, D), while crossings of *act7-4* with lines expressing endosomal/pre-vacuolar markers RabF1/ARA6, Syp22 and Syp61 revealed intracellular localization defects (Supplemental Figure 14).

These findings encouraged us to co-localize ABCB4/ABCB19 and PIN1/PIN2 with different endosomal and vacuolar markers in *act7-4*. ABCB4, ABCB19 and PIN2 (but not PIN1) showed increased co-localization with FM4-64 after long-term treatments (Figure 4A-B)

11

and with the vacuolar marker LTR in *act7-4* (Figure 4C-D), while PIN1 revealed already a high co-localization factor in the isogenic WT background. These data suggest a mislocalization of both classes of auxin exporters on compartments of vacuolar/late endosomal origin in *act7-4.* To address further the nature of these structures, we performed short BFA treatments (25 μM, 1 h) of PIN1-GFP and ABCB19-GFP lines and found that both co-localize with PM marker, FM4-64, on BFA compartments in the WT background and *act7-4*. In *act7-4*, PIN1-GFP and ABCB19-GFP were retained beside on BFA bodies on additional compartments with putative late endosomal-like nature (Supplemental Figure 15). These data support further retention of both classes of auxin exporters on compartments of endosomal/vacuolar origin in *act7-4.*

***twd1* and *act7* show overlapping developmental phenotypes that are caused by defects in polar auxin transport**

Arabidopsis contains eight *ACTIN* genes that are grouped into reproductive and vegetative classes; the latter class contains *ACT2, ACT7, and ACT8* (Kandasamy et al., 2009). *ACT7* mutant combinations are dwarfed, with altered cell and organ morphology, suggesting that ACT7 is involved in root growth, epidermal cell specification, cell division, and root architecture (Kandasamy et al., 2009). The actin defects in *twd1* and auxin transporter de-localizations in *act7* stimulated us to compare in detail auxin-regulated phenotypes in *twd1* and *act7*, with special focus on tissues and processes related to actin-dependent growth.

A hallmark of the *twd1* phenotype is a non-handed, helical rotation (twisting) of epidermal layers that can be (like in *abcb1 abcb19*) partially rescued by NPA treatment (Geisler et al., 2003; Wu et al., 2010; Bailly et al., 2014; Figure 5A). Interestingly, we found that both *act7* alleles and mutant combinations with *act7*, but not *act2-1* or *act8-2*, also show substantial epidermal twisting that was, however, NPA-insensitive (Figure 5A). Next, we analyzed the planar polarity of root hair positioning, which is determined by a concentration gradient of auxin distribution in the root tip (Grebe, 2004). This gradient itself is regulated by upstream events, such as polar placement of ROP (Rho-of-plant) GTPases or auxin transporter activity (Masucci and Schiefelbein, 1994; Grebe, 2004). Surprisingly, *twd1-1* and both *act7* alleles showed a striking apical shift in root hair positioning that was strongest in *act7-4 twd1-1* and *act7-4 act8-2* (Figure 5B). Defects in planar root hair polarity have also been reported very recently for two new *ACT7* alleles shown to influence ROP positioning (Kiefer et al., 2015). In analogy to epidermal twisting, root hair positioning was only mildly disturbed in *act2-1* and *act8-2*. NPA treatment of WT phenocopied *twd1* and *actin* alleles but again *twd1* was found to be widely NPA-insensitive, while *actin* mutants were even

12

partially rescued (Figure 5B).

Finally, we analyzed leaf trichome branching, which usually displays a variation between one and four branches in WT plants (Holweg and Nick, 2004). Both *act7* alleles exhibited a significant shift toward di-branched trichomes (Figure 5C) as previously reported for *act2 act7* double mutants (Kandasamy et al., 2009). Strikingly, *act7-4* and *twd1-1* showed largely identical trichome branching patterns, which were even more radical in *act7 twd1* and *act2 act7*, again resembling NPA treatments (Grebe, 2004).

To link auxin-related phenotypes to actin function, we employed the actin destabilizing and stabilizing drugs, latrunculin B and jasplakinolide, shown to reduce the elongation rate and to induce actin polymerization, respectively (Staiger et al., 2009). Like NPA, latrunculin B and jasplakinolide treatments were able to block apical hook formation in etiolated WT seedlings (Figure 5D) known to be dependent of a local accumulation of auxin at the inner side of the hook (Zadnikova et al., 2010). Interestingly, *twd1* hooks were less sensitive to NPA and latrunculin B treatments than WT but not to jasplakinolide, most probably due to already reduced actin bundling (Figure 2B). *act7-4* was fully responsive to all treatments, further underlining functional redundancy between vegetative actin isoforms (Kandasamy et al., 2009).

Latrunculin B and jasplakinolide had a similar inhibitory effect on hypocotyl elongation as NPA in WT, and like for hook opening, *twd1-1* but not *act7-4* was greatly insensitive (Supplemental Fig. 7A). Interestingly, paclitaxel/ taxol and oryzalin, well-established stabilizers and inhibitors of microtubule polymerization, similarly affected hypocotyl length in *twd1-1* (and *act7-4*) in comparison to WT (Supplemental Fig. 7B) making an involvement of TWD1 (and ACT7) in microtubule-related cell elongation unlikely.

Overlapping auxin-related growth phenotypes between *act7* and *twd1* mutants support a tight mechanistic link between actin dynamics and auxin efflux (Muday, 2000; Blancaflor et al., 2006; Dhonukshe et al., 2008). This stirred us to quantify auxin responses and transport in *act7* mutants. Activation of the auxin-responsive DR5rev:GFP reporter (Friml et al., 2003) was slightly reduced in the *act7-1* allele but more drastically in the *act7-4* root tip, as has been reported before for *twd1-1* (Figure 6A-B; Bouchard et al., 2006). Interestingly, latrunculin B and jasplakinolide treatments phenocopied *TWD1* and *ACT7* loss-of-function, implying that these drugs also cause PAT defects. In agreement, free IAA levels were significantly elevated in *act7-4* and *twd1-1* roots (Figure 6C; Bouchard et al., 2006).

Finally, we employed a self-referencing IAA-specific microelectrode that permits

13

continuous, non-invasive recordings of distinct IAA flux peaks in the epidermis of the apex of *Arabidopsis* roots (Mancuso et al., 2005; Henrichs et al., 2012), correlating with a PIN-dependent auxin 'reflux loop' from peripheral root cells toward central vascular cells (Blilou et al., 2005). Latrunculin B and jasplakinolide treatments (each 5 μM) blocked root PAT as efficiently as NPA (Bailly et al., 2008), which is genetically copied by loss of *ACT7* function (Figure 6D, E). Interestingly, root auxin fluxes into *act7-4* roots show reduced sensitivities to latrunculin B and jasplakinolide (Supplemental Figure 16), resembling *twd1*, which is insensitive to NPA (Bailly et al., 2008).

In summary, these data sets support the concept that either destabilization or stabilization of the actin cytoskeleton causes PAT defects to a similar magnitude as reported for NPA treatments. Overlapping growth phenotypes and PAT defects caused either by chemical actin (de)stabilization or by *TWD1* or *ACT7* mutations suggest that abnormal actin cytoskeleton function in *twd1* is the primary reason for PAT defects, which are likely to be the cause of previously overlooked developmental defects in *twd1*.

Expression of TWD1 in yeast alters budding and actin polarity and confers NPA sensitivity

With the apparent conserved FKBP functionality in mind, we phenotypically characterized WT budding yeast expressing *Arabidopsis* TWD1 and found that these yeasts held a significant higher population of large-budded cells compared to those harboring the vector control, while the amount of un-polarized cells stayed constant (Figure 7A-B). NPA completely reverted this promotional effect of TWD1 on large buds, while the vector control was NPA insensitive. Interestingly, the TWD1^{K79I} mutant shown above to be unable to bind NPA but still to be capable of regulating ABCB1 activity (Supplemental Figure 4) had the same effect on yeast polarization as WT TWD1 but was, as expected, NPA insensitive. However, expression of the strong NPA binder, TWD1^{Q82A}, increased accordingly the number of non-polarized cells but was also NPA insensitive, suggesting that this mutant fails to complete downstream signaling.

In an un-budded cell, actin cables and patches are distributed randomly but during budding, actin cables become bundled and are polarized towards the budding site (Casamayor and Snyder, 2002). To connect the growth phenotypes caused by TWD1 with a putative effect of TWD1 on the yeast cytoskeleton, we quantified the percentage of yeast with polarized actin by staining actin filaments with phalloidin-Alexa Fluor 488. Yeast expressing TWD1 revealed a significantly higher amount of actin polarization in un-budded cells in comparison to the vector control, while actin in large-budded TWD1 cells was less

14

501 polarized (Figure 7C). In agreement with budding analyses, expression of TWD1^{K79I}

502 altered actin polarization in large buds and as expected did not convey NPA sensitivity to

503 this process.

504 An unexpected finding was that expression of TWD1 and TWD1^{K79I} increased the cell size

505 of mother cells and buds significantly, independently from their actin polarization status

506 (Supplemental Figure 17). Surprisingly, increased cell size was exaggerated by NPA

507 treatments, however, in an action that was TWD1-independent.

508 As actin polarization and connected vesicle transport forms the basis for yeast budding,

509 our yeast data provide evidence that growth defects in yeast expressing TWD1 are

510 triggered by altered actin polarization. They also indicate that the effect of TWD1 on the

511 actin cytoskeleton is evolutionarily conserved, as was demonstrated for the function of

512 auxin transport inhibitors on actin (Dhonukshe et al., 2008). However, in this study NPA

513 was less effective in promoting actin bundling in comparison to TIBA or PBA, most

514 probably due to a lack of an appropriate NPA target. Deletion of all four FKBPs, *FPR1-4*, in

515 the yeast strain KDY81.18c (Hemenway and Heitman, 1996) significantly reduced budding

516 (Supplemental Figure 17B) similarly as was found for expression of TWD1^{Q82A}. The

517 finding, however, that size in the *fpr1-4* yeast was not affected by NPA suggests that the

518 effect of NPA on yeast size is provided by yeast-endogenous FKBPs, further supporting an

519 evolutionary conservation of this individual function.

520

521 **DISCUSSION**

522 Inhibitors of auxin export, with NPA being the most prominent, have been widely used in

523 plant biology for almost a century and have greatly contributed to our understanding of the

524 mechanisms of auxin-mediated plant development. Besides inhibiting auxin transport

525 directly, auxin transport inhibitors at higher concentrations also alter actin stability

526 (Rahman et al., 2007; Dhonukshe et al., 2008; this study) and vesicle trafficking (Geldner

527 et al., 2001); however, their mode of action and molecular targets are still remarkably

528 unclear (Luschnig, 2001; Muday and Murphy, 2002; Dhonukshe et al., 2008; Zhu and

529 Geisler, 2015). Finally, it is unknown if the effects of auxin transport inhibitors on the actin

530 cytoskeleton, vesicle trafficking and on auxin transport are directly connected.

531 In this study, we have characterized the FKBP42 TWD1 as a low-affinity binding protein for

532 established auxin transport inhibitors, including NPA. We precisely mapped the NPA-

533 binding surface outside of the putative PPIase/FK506 binding site of the FKBD (Figure 1;

534 Supplemental Figure 2). Drug binding to this subdomain might offer a justification for the

535 atypical structural FKBP clamp (residues S31 to A44) in TWD1 that is thought to be held in

15

place by a stacking interaction between the rings of W77 and P37 (Figure 1B; Burgardt et al, 2012). In agreement, mutation of P37 drastically alters protein stability (Supplemental Figure 3). Notably, the NPA contact region on TWD1 corresponds quite closely to the interaction site in the modeled complex between TWD1 and the second nucleotide-binding domain of ABCB1 (Granzin et al, 2006), providing a mechanistic explanation for the finding that μM concentrations of NPA are sufficient to disrupt TWD1-ABCB1 interaction (Bailly et al, 2008). In summary, it appears as if the N-terminal FKBD might have lost its originally conserved PPIase activity toward a functionality that serves as a platform for multiple protein-protein interactions that are modulated by regulatory drugs, such as NPA.

TWD1 physically and functionally interacts with structural actin cytoskeleton components (here: ACT7; Supplemental Fig. 7 and Supplemental Data set 1). Moreover, our live cell imaging analyses established that TWD1 influences both actin bundling and actin filament dynamics at the cortex of hypocotyl epidermal cells (Figure 2, Table 2). This role for TWD1 and physical interaction with ACT7 is in line with previous *in vitro* and *in vivo* data supporting the concept that a peripheral NPA-binding protein is associated with the cytoskeleton (Cox and Muday, 1994; Dixon et al., 1996; Butler et al., 1998). This holds especially true in light of evidence indicating that TWD1 is attached to the PM via an in-plane membrane anchor (Scheidt et al., 2006; Bailly et al., 2014). Indirect support for this concept also comes from the finding that NPA binding capacities are reduced in both *twd1*, *act7* and *act8* but not in *act2* (Figure 1E), which – based also on our phenotypical analyses (Figure 5) - seems to own a distinct function. Recently, ACT2 was shown to integrate BR signaling and BR-mediated auxin responses (Lanza et al., 2012). A distinct functionality for ACT2 is further supported by the finding that *act2-5* roots revealed reduced actin filament skewness similar to brassinosteroid or auxin treatments (Lanza et al., 2012), while *act7-4* and NPA treatments had opposite effects (Figure 2).

Stabilization of actin bundles and thus regulation of vesicle dynamics by several auxin transport inhibitors is conserved among plant, yeast and mammalian cells (Dhonukshe et al., 2008). In agreement with our data (Figure 7), previous work failed to demonstrate an effect on actin bundling for NPA in yeast, while PBA and TIBA were effective (Dhonukshe et al., 2008). Expression of TWD1 specifically fostered yeast budding most likely as a consequence of TWD1-mediated polarization of actin filaments (Figure 7), serving as cargo tracks for polar vesicle delivery to new buds (Casamayor and Snyder, 2002). Importantly, this action was reverted by NPA, while vector-control yeast were NPA insensitive, indicating that TWD1 is responsible for NPA sensitivity (Figure 7). Further

571 support is provided by the fact that the non-NPA binder, TWD1[K79I], widely retains its ability
572 to regulate actin polarization and yeast budding but does not confer NPA sensitivity,

573 In agreement with an actin filament bundling role for TWD1, the PM presence of auxin
574 efflux transporters is seriously distorted in *twd1* (Wu et al., 2010; Wang et al., 2013) but
575 also in *act7* (Figures 3-4). While the role of TWD1 as a chaperone during ER to PM
576 secretion seems to be specific for ABCBs (Bouchard et al., 2006; Wu et al., 2010; Wang et
577 al., 2013), both PINs and ABCBs are retained at early endosomal/vacuolar compartments
578 in *act7* (Figure 4). Based on marker and BFA analyses, *act7* has severe defects in
579 endosomal balance, which affect expression and PM location of all tested ABCBs and
580 PIN2 with ABCB4 being the most disturbed, while PIN1 was only mildly concerned
581 (Figures 3-4; Supplemental Fig. 15). A more drastic perturbation of PM trafficking in *act7* is
582 to be expected from the genetic loss of a structural actin cytoskeleton component, which
583 should have more severe consequences on transporter trafficking than the loss of a
584 bundling activity provided by TWD1.

585 Our data also provide a mechanistic explanation of why treatment of Arabidopsis roots with
586 TIBA and NPA prevents the BFA-induced internalization of PIN1 and the trafficking of
587 internalized PIN1 to the PM after BFA washouts (Geldner, et al., 2001). The NPA
588 concentration needed to reduce PIN1 cycling was 200 μM (Geldner et al., 2001), which is
589 in agreement with our *in vitro* NPA binding affinities found for TWD1. Our data now also
590 provide a rationale for the NPA sensitivity of ABCB4-GFP localization in epidermal cells
591 (Kubes et al., 2012).

592 We further show that actin filament unbalancing (caused by pharmacological actin
593 stabilization or destabilization) can block PAT to the same degree as NPA or loss of *ACT7*
594 (Figure 6), resulting in similar phenotypic defects, exemplified here by hook opening
595 (Figure 5). Therefore, our data provide further evidence that the actin cytoskeleton plays a
596 direct role in PAT and that TWD1 functions as an integrating node of actin cytoskeleton
597 organization/dynamics, vesicle trafficking and PAT and mediates the action of NPA in these
598 processes (Supplemental Figure 18). As a proof of concept, auxin-triggered physiology,
599 such as root gravitropism, hypocotyl elongation, root hair positioning and hook opening,
600 but also actin filament organization and dynamics are largely not affected by NPA in *twd1*.
601 Further indirect validation comes from the finding that *act7* and *twd1* mutants show
602 overlapping developmental phenotypes that are dependent on local auxin gradients
603 (Figure 6).

604 Our findings obviously also support the hypothesis that auxin regulates its own transport
605 by unbundling actin filaments (Nick et al., 2009; Zhu and Geisler, 2015) and that auxin

transport inhibitors counteract this response through actin bundling, which is regulated by TWD1. However, it is important to recall that auxin transport inhibitors, such as NPA, are synthetic compounds for which the potential *in planta* counterparts are not known. Based on NPA displacement (Jacobs and Rubery, 1988), flavonols were originally discussed to work as plant-endogenous auxin transport inhibitors (Peer and Murphy, 2007). However, although flavonols efficiently disrupt TWD1-ABCB interaction (Bailly et al., 2008), based on our findings presented here (Supplemental Figure 1) flavonols seem unlikely to work via TWD1.

Although previous studies have established that ATI modulates actin bundling (Dhonukshe et al., 2008; Zhu and Geisler, 2015), underlying mechanisms have not been investigated in detail. Here, we quantitatively resolved how NPA modifies various parameters of single AF dynamics (Table 2), and provide mechanistic insight into how TWD1 ultimately stimulates the overall actin bundling level in hypocotyls (Figure 2). Most importantly, our data revealed that NPA decreases AF dynamics/turnover (as indicated by increased AF lifetime and length) in a process involving both an increase of the elongation rate and a decrease of the severing frequency (see Table 2). This effect likely accounts for the overall increase of actin bundling observed in NPA-treated hypocotyls (Supplemental Figure 18B) since NPA does not act by increasing the AF bundling frequency (see Table 2). Remarkably, the various effects of NPA on single AF parameters were all abrogated in *twd1-1* mutants (Table 2), indicating that TWD1 is a key mediator of NPA action on AF dynamics. The finding that the *twd1-1* mutant exhibits defects in single AF parameters similar to those induced by NPA and resulted in a reduced turnover of AFs (see Table 2), suggests a model where NPA inhibits this TWD1-mediated activity (axis 1 in Supplemental Figure 18B). Besides promoting AF de-stabilization, we found that TWD1 strikingly lowers the frequency of actin de-bundling (see Table 2). This additional regulatory axis likely strengthens the increase of the overall actin bundling level in NPA-treated hypocotyls in a context where the actin dynamizing activity of TWD1 is blocked (Supplemental Figure 18B). NPA inhibits actin de-bundling apparently in a TWD1-independent manner; therefore, the regulatory components involved remain an open question.

Based on the outcome that TWD1 most likely does not autonomously bind to actin and directly control AF dynamics (Supplemental Figure 9), we propose third-party actin-binding proteins as functional linker candidates (Thomas, 2012; Zhu and Geisler, 2015). The complex effect of TWD1 on AF organization and dynamics (*i.e.* a combined increase in actin dynamics and reduction in de-bundling) argues for the idea that TWD1 functionally interacts with two (or more) independent regulatory actin-binding factors (Supplemental

Figure 18B). According to this model, root-shoot-specific expression of TWD1-controlled regulatory actin binding proteins might account for the confusing opposite effects of auxin transport inhibitors on the overall actin cytoskeleton organization in roots and shoots (Rahman et al., 2007; Supplemental Figure 10). Importantly, like in hypocotyls, NPA action in roots requires TWD1, as indicated by the inability of NPA to increase the overall actin bundling level in *twd1-1* roots (Supplemental Figure 10). As expected, overall actin bundling in *act7-4* hypocotyls is NPA insensitive (Fig. 2, Supplemental Figure 10A-B); however, this is apparently not the case in roots (Supplemental Figure 10C-D). Further, unlike *act7-4* hypocotyls that reveal enhanced AF bundling compared to the WT, root overall actin bundling is reduced (Supplemental Figure 10C-D). These findings argue for an involvement of root/shoot-specific actin binding proteins.

Potential TWD1-ACT7 linker candidates might belong to formin or villin families of actin-binding proteins, which regulate actin organization and dynamics (Henty-Ridilla et al., 2013; Zhu and Geisler, 2015). For instance, Rice Morphology Determinant (RMD), a type II formin, was shown to link auxin-actin regulation by influencing cell growth (Li et al., 2014). Moreover, very recently, down-regulation of the three vegetative profilins, PRF1-3, was reported to result in a drastic dwarfed phenotype resembling *twd1* (Mussar et al., 2015). Finally, Arabidopsis *vln2 vln3* and rice *vln2* mutants show a twisted disorientation of organs (van der Honing et al., 2012; Wu et al., 2015). For the rice *vln2* mutant, it was shown that developmental defects correlate with altered actin dynamics causing PIN2-delocalization and PAT defects (Wu et al., 2015). Future work should establish the exact nature of the actin-binding proteins involved in TWD1-mediated regulation of polar auxin transport.

METHODS

NMR spectroscopy

^{15}N-labelled TWD1$^{1-180}$ from *Arabidopsis thaliana* was prepared as previously described (Kamphausen et al, 2002), except that the BL21 codon+RIL cells (Stratagene, La Jolla, USA) were grown at 30°C in M9 minimal medium with ^{15}N-NH$_4$Cl as the sole nitrogen source and harvested 3h after induction with 0.5 mM isopropyl-β-D-thiogalactopyranoside (IPTG). NMR samples contained 0.7 mM ^{15}N-labelled FKBP42$^{1-180}$ in 10 mM Na$_2$HPO$_4$ buffer (5% D$_2$O, 3% DMSO-d$_6$, pH 7.0). For the chemical shift perturbation experiments, the TWD1$^{1-180}$ samples were supplemented with NPA (3.1 mM) or quercetin (0.7 mM), each administered in DMSO-d$_6$. pH of all samples was controlled by a pH electrode before and after the NMR measurements, and adjusted wherever needed.

NMR spectra were acquired at 25°C using a Bruker DRX500 spectrometer operating at

19

500.13 MHz proton resonance frequency and equipped with a 5 mm triple-resonance $^1H/^{13}C/^{15}N$ probe with gradient capability. Heteronuclear 2D $^1H/^{15}N$-HSQC spectra were collected with the carrier placed in the center of the spectrum on the water resonance, which was suppressed by applying a WATERGATE sequence. Quadrature detection in the indirectly-detected dimension was obtained by the States-TPPI method. All NMR spectra were acquired and processed on Silicon Graphics computers using the program XWINNMR 3.5 (Bruker Bio-Spin, Rheinstetten, Germany). A 90° phase-shifted squared sine-bell function was used for apodization in all dimensions. Polynomial baseline correction was applied to the processed spectra in the directly-detected ^1H dimension. The chemical shifts were referenced to external DSS in order to ensure consistency among all spectra. Spectra were analyzed with SPARKY 3 (University of California, San Francisco, USA). Chemical shift differences in the amide proton ($\Delta\delta_{1HN}$) and nitrogen ($\Delta\delta_{15N}$) resonances of the free and complexed protein forms were combined for each residue by using the expression $[(\Delta\delta_{1HN})^2 + (\Delta\delta_{15N}/6.5)^2]^{1/2}$.

Quantum chemical modeling

A theoretical examination of the geometry, electronic structure, and electronic binding energies (ΔE) of the putative NPA binding pocket of TWD1 was performed using data from the crystal structure of the TWD1 FKBD (PDB accession code 2IF4). The orientations of the NPA molecule on the TWD1 binding surface were examined by molecular dynamic calculations using OPLS force fields. Next, the energetically most stable NPA bound conformation in the TWD1 pocket (~500 atoms) was found by optimizing different geometries using Density Function Theory calculations including the Van der Waals correction D3 (DFT-D) with the bp86 functional and double-zeta polarized atomic basis set level (def-SV(P)). The selection of the NPA cavity considered previous analyses of auxin molecules (Ferro et al, 2006), protein cavities (Rolo-Naranjo et al, 2010) and the NMR information. All calculations were performed with GROMACS (http://www.gromacs.org/) and TURBOMOLE (http://www.turbomole.com).

Computational chemistry experiments were conducted to analyze the influence of the substitution mutants P37L, K39I, K79I, Q82A and H125I. Their geometries were re-optimized at DFT-D level with bp86 and the D3-correction. The re-optimizations included both pocket–NPA pairs as well as NPA and pockets alone. Their binding forces were calculated according to the general equation $\Delta E_{cal}=\Delta E_{pocket - NPA} - (\Delta E_{pocket} + \Delta E_{NPA})$ using the accurate MGGA-based hybrid exchange-correlation *functional* (TPSSH) and TZVP as basis set. The thermochemical analysis considered an average binding energy,

711 ΔP_{ave}, that consists of $\Delta E_{ave} = \Delta E + \Delta E_{VdW} + \Delta E_{def}$ with the following parameters: effects of

712 electronic binding energies (ΔE), Van der Waals forces (ΔE_{VdW}) and deformation energies

713 of the protein (ΔE_{def}). The calculations solved the electronic problem of the interaction of

714 NPA on the TWD1 protein surface pocket accurately and allowed calculations of average

715 binding and further analysis of the potential surface and electronic density using the theory

716 of deformed atoms in molecules (DAM; Fernandez Rico et al., 2004).

717 ΔE values from QM analysis were approximately transformed into ΔG values using the

718 equation RT ln (ΔU) without taking into account the direct estimation of solvation (ΔG_{sol})

719 and entropic effects (TΔS), which is given as follows: $\Delta G = \Delta G_{sol} + \Delta U - T\Delta S$.

720

721 **In silico substrate docking to TWD1**

722 One thousand poses for NPA and benzoic acid (BA) were generated using the PyMOL

723 embedded AutoDock Vina toolset (Seeliger and de Groot, 2010) as described in (Bailly et

724 al., 2012). To avoid any bias, the search space was first defined as the whole rigid TWD1

725 (PDB 2IF4; Granzin et al., 2006) structure with high exhaustiveness (Supplemental Figure

726 2). Calculations were further refined to the FKBD (FK506-binding domain; PDB 2F4E;

727 Weiergraber et al., 2006) in flexible side-chain mode for the whole FKBP42[34-180] segment

728 and resulted in 10 clusters with close conformations (Supplemental Figure 2).

729

730 **Affinity purification of TWD1-CFP interacting proteins and mass spectrometric**

731 **analysis**

732 Co-immunoprecipitation analyses were carried out in triplicate as described recently

733 (Henrichs et al., 2012) except that bands of interest were size-selected by silver stain and

734 manually cut out of the gel prior to trypsin digest. LC-MS/MS analyses were performed by

735 using an LTQ-Orbitrap XL-HTC-PAL system. MS/MS spectra were analyzed using the

736 MASCOT server (version 2.2) searching the TAIR10 database (The Arabidopsis

737 Information Resource). The MASCOT search parameters were as follows: set off the

738 threshold at 0.05 in the ion-score cut off, peptide tolerance at 10 ppm, MS/MS tolerance at

739 ± 0.8Da, peptide charge of 2+ or 3+, trypsin as enzyme allowing up to one missed

740 cleavage, carboxymethylation on cysteines as a fixed modification and oxidation on

741 methionine as a variable modification. Mascot identified vector control proteins were

742 subtracted manually from TWD1-CFP proteins, and proteins were sorted according to their

743 appearance in triple experiments (identified counts) and listed according to their score

744 (Supplemental data set 1). Mascot identified proteins from three independent co-IP/MS

745 analyses were classified according to their putative biological process, their cellular

21

746 components and their molecular function using Blast2Go (www.blast2go.com).

747

748 **In vitro TWD1-actin interaction analyses**

749 Binding of TWD1$^{1\text{-}339}$ and TWD1$^{1\text{-}180}$ (FKBD) proteins to rabbit actin filaments was

750 assessed in high-speed co-sedimentation assays. Briefly, increasing amounts (0.2 – 8 µM)

751 of TWD1$^{1\text{-}180}$ (Weiergraber et al., 2006) or TWD1$^{1\text{-}339}$ protein (Granzin et al., 2006) were

752 incubated with pre-polymerized F-actin (4 µM) under different pH conditions in the

753 presence or absence of CaCl$_2$ (+/- 303 µM) and centrifuged at 150,000 g (Hoffmann et al.,

754 2014a). The resulting pellet and supernatant fractions were analyzed by SDS-PAGE and

755 Coomassie Blue staining (or immunoblot analyses using anti-TWD1 (Wang et al., 2013)).

756 The influence of TWD1 on AF polymerization kinetics was investigated in classical

757 fluorimetric assays using pyrene-labeled actin filaments (3 µM) with 12 µM TWD1$^{1\text{-}339}$ +/-

758 12 µM NPA (Hoffmann et al., 2014a). The increase in pyrene fluorescence accompanying

759 actin polymerization was recorded over 1000 s using a PTI QM-4 QuantaMaster

760 fluorimeter.

761

762 **Drug binding studies**

763 Drug binding assays using *Arabidopsis* or yeast microsomes were performed as described

764 elsewhere (Bailly et al., 2008). Four replicates of 20 µg protein each were incubated with

765 10 nM radiolabelled NPA (ARC Inc., St. Louis, USA; 60 Ci/mmol) in the presence and

766 absence of 10 µM non-radiolabelled NPA. Reported values are the means of specific

767 radiolabeled drug bound in the absence of cold drug (total) minus radiolabelled drug

768 bound in the presence of cold drug (unspecific) from at least three independent

769 experiments with four replicates each.

770 TWD1 was expressed in WT yeast strain JK93da (Hemenway and Heitman, 1996) from

771 shuttle vector pRS314CUP:TWD1-Rluc (Bouchard et al., 2006). Point mutations in TWD1

772 (TWD1^{K39I} , TWD1^{K79I} , TWD1^{H125I} and TWD1^{Q82A}) were introduced using the QuikChange

773 XL site-directed mutagenesis kit (Stratagene, La Jolla, CA).

774 NPA, TIBA, BUM and BA binding of TWD1 was assayed by Surface Plasmon Resonance

775 (SPR) on a Reichert SR7500DC instrument (Reichert Technologies, Depew, NY). Ligand

776 protein (TWD1$^{1\text{-}339}$ in 10 mM sodium acetate buffer pH 5) was immobilized on

777 carboxymethyl dextran hydrogel sensor chips (CMD500m, XanTec Bioanalytics GmbH,

778 Düsseldorf, Germany) to variable levels (15000-19000 uRIU) by thiol and amine coupling

779 according to manufacturers' instructions (GE Medical Systems AG, Glattbrug, Schweiz;

780 XanTec Bioanalytics GmbH, Düsseldorf, Germany). Analyte (NPA, BUM, TIBA and BA)

22

stock solutions (10 mM) and dilution series were prepared in EtOH and diluted into running buffer (10 mM HEPES, 150 mM NaCl, 10 mM MgCl$_2$, 10 mM KCl, 0.005% Tween-20, 1 % EtOH, pH 7.6) before addition of EtOH. For each experiment at least three independent dilutions of analyte at the indicated concentrations were injected in duplicates, first over the immobilized ligand surface and subsequently over an L-cysteine (thiol coupling) or ethanolamine (amine coupling)-blocked reference channel at a flow speed of 20 μL/min. No ligand regeneration was required due to fast and complete analyte dissociation. Base line drift was minimal within experiments and effects of mass transport were excluded in initial trials. Association and dissociation of the analytes were monitored for 120 s each. All experiments were carried out at 25°C and included running buffer injections for double referencing. Double referencing and data analysis was performed using Scrubber2 (BioLoglic Software Pty Ltd, Campbell, Australia) and Tracedrawer (Ridgeview Instruments, Vänge, Sweden) analysis software, respectively. Obtained sensogramms were globally fitted with inclusion of a parameter correcting for local bulk index changes using a 1:1 Langmuir binding model (thiole coupling) or 1:2 surface heterogenicity model (amine coupling) for evaluation of kinetic parameters. ka, kd and K$_{D(kin)}$ K$_{D(eq)}$ were obtained from response data collected at near Equilibrium towards the end of the injection and analyzed in Tracedrawer (Ridgeview Instruments AB, Vänge, Sweden) using the Affinity/EC50 tool. ΔG° was calculated using the formula ΔG°=RT ln K$_D$. All experiments were repeated at least 3 times on independent sensor chips.

Confocal laser scanning and variable angle epifluoresence microscopy
For confocal laser scanning microscopy work, Leica TCS SP2, Leica TCS SP5 or Zeiss LSM780 equipment was used. Various confocal settings were set to record the emission of GFP (excitation 488 nm, emission 500–550 nm), CFP (excitation 458 nm, emission 468–500 nm), FM4-64 and LTR (excitation 543 nm, emission 580–640 nm). Whole-mount immunolocalizations in 5 dag *Arabidopsis thaliana* roots were carried out as described (Friml et al., 2003). Images were acquired with the Leica confocal software 2.00 using identical settings for all samples. Antiserum concentrations were as follows: anti-TWD1 (1:500; Wang et al., 2013), anti-ARF1 (1:600; Agrisera; as08325) and CY3-conjugated anti-rabbit (1:600; sheep anti-rabbit IgG, Sigma Aldrich; C2306). Polyclonal anti-PIN1 (1:500) and anti-PIN2 (1:500) were raised in rabbits against amino acid epitopes 227-383 and 189–477, respectively as described in Abas et al. (2006) and Friml et al. (2003). Indicated peptides were expressed from vector pDEST17 and purified as N-terminally 6xHis-tagged versions as described in Friml et al. (2003). Short (2 μM, 15 min) and long-

term (4 μM, 3 h) FM4-64 (ThermoFisher; T3166), lysotracker red (LTR; ThermoFisher; L7528) (2 μM, 60 min), brefeldin A (BFA; Sigma Aldrich; B7651) (25 μM, 1 h) treatments were carried out as described elsewhere (Wang et al., 2013).

For analysis of skewness in hypocotyls or roots of 5 dag GFP-fABD2 lines, we used Leica TCS SP5 and Zeiss LSM780 confocal microscopes, respectively. An approach similar to that of Higaki et al. (2010) generating maximum projections of static image stacks, applying Gaussian blur at 1.0 px radius and skeletonizing with the ThinLine function of the Kbi_2d-filter package plugin (http://hasezawa.ib.k.u-tokyo.ac.jp/zp/Kbi/KbiFilter2d) was employed. All actin image analyses were performed in the FIJI distribution of ImageJ 1.46a (http://imagej.nih.gov/ij/). Skewness parameters were obtained by the line features function of the package for the entire frame, comprising pictures of at least eight hypocotyls or roots. At least 60 cells were measured.

Variable angle epifluorescence microscopy (VAEM) imaging of the cortical cytoplasm of epidermal cells was essentially as described in (Hoffmann et al., 2014b). Illumination was achieved using a total internal reflection fluorescence (TIRF) illuminator mounted on an Axiovert 200 M microscope equipped with a 100 x 1.46 NA TIRFM PlanApo objective (Zeiss). After focusing on the first visible actin filaments at the periphery of a cell, the angle of laser illumination was adjusted for maximal contrast and signal-to-noise ratio. We estimate the depth of focal plane at 0.5–1 µm in VAEM mode. Illumination was from a 100-mW argon ion laser (attenuated to 5% power with neutral density filters and shuttered between consecutive exposures. The 488-nm laser line was filtered through a BP filter (N°52; Zeiss) and GFP emission from the specimen captured with a 512 × 512 electron-multiplying CCD camera (AxioCamHR3; Zeiss). Typical exposure times were around 600 ms.

For quantitative analyses, time-lapse series of around 100 images were collected at 2–3 s intervals and a table of elapsed time between each frame recorded. Cropped regions and subsets of the time-lapse images were converted to 7 frames per second (fps) QuickTime movies, without compression. To measure actin filament lengths, elongation rate and severing frequency, actin filaments were tracked manually through the time-lapse stack of images as described in detail in (Staiger et al., 2009). For filament lifetime the definition of Henty et al. (2011) was used. Actin bundling and de-bundling frequencies were analyzed as in Hoffmann et al. (2014) and Zheng et al. (2013). At least 100 filaments from at least 20 different cells in 10 or more hypocotyls were selected. All single actin filament quantifications have been analyzed in double-blind analyses in order to avoid any bias.

Auxin transport

A platinum microelectrode was used to monitor IAA fluxes in *Arabidopsis* roots as described previously (Mancuso et al., 2005). For measurements, WS WT plants (WT) or *act7-4* were grown in hydroponic cultures and used at 5 dag. Differential current from an IAA-selective microelectrode was recorded in the absence and presence of 5 μM NPA, jasplakinolide or latrunculin B.

In planta analysis of auxin contents and responses

Endogenous free IAA was quantified from MeOH extracts of seedlings shoot and root segments using gas chromatography-mass spectrometry (GC-MS) as described in (Bouchard et al., 2006). Data are means of four independent lots of 30–50 seedlings each, and equivalent to ca. 30 mg root and 60 mg shoot material, respectively.

Homozygous generations of *A. thaliana act7-1/4*, *twd1-1* and *act7-4 twd1-1* seedlings (generated by crossing) were obtained by transformation with DR5$_{rev}$:GFP (Ottenschlager et al., 2003). Seedlings were grown vertically for 5 dag and transferred O/N on 500 nM jasplakinolide or 20 nM latrunculin B plates and analyzed by confocal laser-scanning microscopy.

Plant Material and Phenotypic Analyses

The following *Arabidopsis thaliana* lines in ecotype Wassilewskija (WS WT) were used: *abcb1-1 (At2g36910), abcb19-1 (At3g28860)* and *abcb1-1 abcbb19-1* (Noh et al., 2003); *twd1-1* (At3g21640); Geisler et al., 2003); *act7-1 (At5g09810), act7-4 (At5g09810), act2-1 (At3g18780), act8-2 (At1g49240), act2-1 act7-1, act7-4 act8-2* (Kandasamy et al., 2001; Gilliland et al., 2003); *TWD1:TWD1-CFP* (Wu et al., 2010); *ABCB1:ABCB1-GFP* and *ABCB19:ABCB19-GFP* (Mravec et al., 2008). *Pin2/eir1-4* (At5g57090; Luschnig et al. 1998); *twd1-3* (Geisler et al., 2003); *pin1-1* (At1g73590; Okada et al., 1991); *abcb19-3* (Lewis et al., 2007); *abcb1-100 abcb19-3* (Wu et al., 2010); *ABCB4:ABCB4-GFP* (At2g47000; Cho et al., 2007), 35S:HA-TWD1 (Geisler et al., 2003), *PIN1:PIN1-GFP* and *PIN2:PIN2-GFP* (Abas et al., 2006), GFP-fABD2 (Sheahan et al., 2004); DR5:GFP (Ottenschläger et al., 2003) were all in the Columbia WT (Col-0). *ABCB1:ABCB1-GFP*, *ABCB4:ABCB4-GFP*, *ABCB19:ABCB19-GFP*, *PIN1:PIN1-GFP*, *PIN2:PIN2-GFP*, *TWD1:TWD1-CFP*, *DR5$_{rev}$:GFP* and *35S:GFP-fABD2* transgenic lines were crossed into *act7-4* or *act7-6* (SALK_131610; Kiefer et al. 2015), and isogenic, homozygous lines for the transgene in the F3 generations were used for further analyses; the same strategy was used for the *act7-4 twd1-1* crossing. In case non-isogenic lines were used for analyses

886 (see Fig. 3) artifacts caused by ecotype mixes were excluded by immunolocalizations or
887 employing isogenic controls (Supplemental Figure 13).

888 Seedlings were generally grown on vertical plates containing 0.5 Murashige and Skoog
889 media, 1% sucrose, and 0.75% phytoagar in the dark or at 8 h (short day), 16 h (long day),
890 or 24 h (constant) light per day. Developmental parameters, such as root gravitropism,
891 hook opening, root hair positioning, trichome branching and hypocotyl lengths were
892 quantified by microscopy as described in (Masucci and Schiefelbein, 1994; Wang et al.,
893 2013). Inhibitor concentrations were 400 nM jasplakinolide, 50 nM latrunculin B and 5 µM
894 NPA. Root orientation of epidermal layers to the growth direction (twist angle) were
895 quantified microscopically using agarose imprints as described in (Wang et al., 2013). IAA-
896 induced hypocotyl elongation was performed as in (Schenck et al., 2010). All experiments
897 were performed at least in triplicate with 30 to 40 seedlings per each experiment.

898

899 **Yeast polarity analyses**
900 TWD1 was expressed from shuttle vector pRS314CUP-TWD1 (Bouchard et al., 2006) in
901 WT strain JK93da (Hemenway and Heitman, 1996). Yeast growth, cell polarity and actin
902 polarity was quantified in WT and KDY81.18c strain (Hemenway and Heitman, 1996) as
903 described in (Yu et al., 2011). To characterize the reorganization of actin cables during the
904 cell cycle, cells were divided into three categories based on the size of daughter cells.
905 These categories were un-polarized/unbudded cells (UB), polarized to small-medium
906 budded cells (MB) and large budded cells (LB). All data were derived from a minimum of
907 three independent transformants.

908

909 **Data Analysis**
910 Data were statistically analyzed using Prism 6.0 (GraphPad Software, San Diego, CA).

911

912 **Accession Numbers**
913 Sequence data from this article can be found in the Arabidopsis Genome Initiative or
914 GenBank/EMBL databases under the following accession numbers: ABCB1 (At2g36910),
915 ABCB4 (At2g47000), ABCB19 (At3g28860), TWD1 (At3g21640), ACT1 (At5g09810),
916 ACT2 (At3g18780), ACT7 (At5g09810), ACT8 (At1g49240), PIN1 (At1g73590), PIN2
917 (At5g57090).

918

919 **SUPPLEMENTAL DATA**
920 **Supplemental Figure 1: Superimposed ^{1}H/^{15}N-HSQC spectra showing the backbone**

amide signals of TWD1$^{1-180}$ in the presence of NPA and quercetin in comparison to the solvent.

Supplemental Figure 2: *In silico* docking and quantum chemical modeling of NPA and benzoic acid binding on TWD1.

Supplemental Figure 3: Structural analysis of wild-type and mutant versions of the TWD1 FKBD using Quantum chemical modeling (DFT).

Supplemental Figure 4: NPA binding and regulatory effects of wild-type and mutated versions of TWD1 in yeast.

Supplemental Figure 5: Sensograms and representative fitted models of kinetic analyses and equilibrium analyses of surface plasmon resonance analyses of NPA, benzoic acid, BUM and TIBA binding using thiol-immobilized TWD1$^{1-339}$.

Supplemental Figure 6: Root gravitropism and auxin-induced hypocotyl elongation of *twd1-3* is less sensitive to NPA.

Supplemental Figure 7: Functional classification of TWD1-interacting proteins identified by co-immunoprecipitation followed by MS/MS analyses using TWD1:TWD1-CFP as a bait.

Supplemental Figure 8: TWD1 does not autonomously bind to mammalian actin filaments and affect actin polymerization.

Supplemental Figure 9: Confocal microscopy analyses of cortical actin bundling of hypocotyls and roots expressing GFP-fABD2 treated with 10 μM NPA.

Supplemental Figure 10: Concentration dependency of NPA treatments causing bundling of cortical actin in hypocotyls.

Supplemental Figure 11: Hypocotyl length of *twd1-1* and *act7-4* in the presence and absence of actin and microtubule stabilizing and destabilizing agents.

Supplemental Figure 12: *act7* single and double mutants reveal endosomal and vacuolar defects

Supplemental Figure 13: Expression and localization of PIN and ABCB-type auxin transporters are dependent on ACT7.

Supplemental Figure 14: Endosomal markers, Syp22, Syp61 and RabF2b, are delocalized in *act7-4* compared to the corresponding wild type.

Supplemental Figure 15: ABCB19 and PIN1 co-localize with endocytic marker FM4-64 after BFA treatment.

Supplemental Figure 16: Heat map presentation and influx profiles of IAA influx along wild type, *twd1-1* and *act7-4* roots treated with 5 μM latrunculin B, jasplakinolide or the solvent.

Supplemental Figure 17: Analyses of FKBP action in yeast.

Supplemental Figure 18: Working model summarizing the function of FKBP42/TWD1 as an integrator of actin bundling and polar auxin transport.

Supplemental Data set 1: TWD1 interacting proteins identified by co-immunoprecipitation followed by MS/MS analyses using TWD1-CFP as bait.

Supplemental Movies 1-6: Movies of time-lapse variable angle epifluorescence micrososcopy (VAEM) analyses of representative epidermal hypocotyl cells showing cortical actin labeled by fABD2-GFP of WT (Supplemental Movies 1 and 4), *twd1-1* (Supplemental Movies 2 and 5) and *act7-4* (Supplemental Movies 3 and 6) in the absence (solvent controls, Supplemental Movies 1-3) and presence of NPA (1 μM, 5 dag; Supplemental Movies 4-6).

AUTHOR CONTRIBUTIONS

Conflict of interest

Abbreviations

ABCB, ATP-binding cassette protein subfamily B; AF, actin filament; dag, day(s) after germination; IAA, indole-3-acetic acid; NBP, NPA-binding protein; NPA, 1-*N*-naphthylphthalamic acid; PAT, polar auxin transport; PBA, 2-(1-pyrenoyl) benzoic acid; PID, PINOID; PIN, pin-formed; SPR, surface plasmon resonance; TIBA, triiodobenzoic acid; VAEM, variable angle epifluorescence microscopy; WT, wild-type.

FIGURE LEGENDS

Figure 1: TWISTED DWARF1 (TWD1) is a low-affinity NPA binding protein

(**A**) NMR chemical shift perturbation (CSP) analysis of NPA binding to TWD1[1-180] revealing combined ^{1}H and ^{15}N chemical shift changes. Relevant residues for the binding of NPA above 0.005 ppm are colored according to the legend in (B).

(**B**) Most stable quantum chemical modeling-derived NPA-bound conformations (balls and sticks) correlate with the mapping of CSP values on FKBP42[34-180] (PDB ID 2IF4, color code reflects CSP shifts). Side chains of residues assumed to participate in the binding

29

surface are depicted as sticks; relevant TWD1 mutations are in red. Theoretical FK506-binding to the non-canonical PPIase domain (PDB 1FKJ) is indicated in magenta; W77 and P37 thought to build a stacking interaction are colored in green.

(C) Quantum chemical analysis of the electron density components responsible for the Van der Waals forces between NPA and the surrounding amino acids. Electronic density deformation for NPA (dipole-type deformation in grey and quadrupole-type deformation in black) and for the amino acid residues (dipole-type deformation in orange and quadrupole-type deformation in red; see also Supplemental Figure 3).

(D) Kinetic analysis of NPA binding to thiol-immobilized TWD1[1-339]. Sensograms of injections of 15 μM, 30 μM, 60 μM and 90 μM NPA in color and representative kinetic fit models (1:1) indicated in black. Data is representative for 3 independent experiments with comparable results (see Table 1). Residuals and goodness-of-fit are indicated in Supplemental Figure 5.

(E) Specific ^{3}H-NPA binding calculated as difference between total and unspecific NPA binding determined in the absence (total) and presence of a 1000-fold access of non-radiolabelled NPA concentrations (unspecific). Significant differences (unpaired *t*-test with Welch's correction, $P < 0.05$) from corresponding WS and Col-0 wild types (WT), respectively, are indicated by 'a'.

Figure 2: Actin architecture and NPA sensitivity is altered in *twd1*.

(A-C) Time-lapse variable angle epifluorescence microscopy (VAEM) analyses of cortical actin of dark-grown hypocotyl expressing fABD2-GFP treated with 1 μM NPA. Representative epidermal cells (**A**) and quantification of actin bundling (skewness, **B**) and percent occupancy (density, **C**); bar, 10 μm. Significant differences (unpaired *t* test with Welch's correction, $p < 0.05$) between wild type (WT) and mutant alleles are indicated by 'a', significant differences to solvent controls by 'b' (mean ± SE; $n \geq 100$).

Figure 3: ACT7 regulates ABCB and PIN-type auxin transporter and TWD1 expression and location.

(A-B) Auxin transporters, ABCB1,4,19-GFP **(A)** and PIN1,2-GFP, as well as the ABCB chaperon, TWD1-CFP **(B),** are delocalized from the root PM and ER, respectively, and retained on punctuated structures (arrows) and are significantly down-regulated in *act7-4* in comparison to the corresponding WT lines. Bars, 10 μm.

(C) Quantification of **(A-B).** Significant differences (unpaired *t* test with Welch's correction,

p < 0.05) between wild type and *act7-4* are indicated by 'a' (mean ± SE; n ≥ 50 images). Note that GFP quantifications by confocal imaging were performed over identically defined areas of the entire root tip and therefore quantified intensities in (C) might not match pictures in (A-B). Further, that for PIN1,2-GFP and ABCB4-GFP non-isogenic lines were used for analyses in *act7-4* but that artifacts caused by ecotype mixes were excluded by immunolocalizations or isogenic controls (Supplemental Figure 13).

Figure 4: ABCB and PIN-type auxin exporters co-localize with vacuolar markers in *act7-4*.

(A) ABCB4-GFP, ABCB19-GFP, PIN1-GFP and PIN2-GFP co-localize (arrows) with compartments stained after long FM4-64 treatments (4 μM, 3 h) in *act7-4* indicating vacuolar origin. **(C)** ABCB19 and PIN1, and to a lesser extent ABCB4 and PIN2, co-localize with late vacuolar marker, lysotracker red (LTR), in *act7-4*. Bars, 10 μm.

(B, D) Quantification of ABCB and PIN co-localization in WT and *act7-4* with FM4-64 **(B)** and LTR markers **(D).** Significant differences (unpaired *t* test with Welch's correction, p < 0.05) between wild type and *act7-4* are indicated by 'a' (mean ± SE; n ≥ 50 images).

Figure 5: *twd1* and *act7* show overlapping developmental phenotypes

(A) *act7-4* like *twd1-1* shows a reduction in growth (upper panel; scale bar, 2 cm) and a significant disorientation of epidermal layers to the growth direction (twist angle, lower panel). Significant differences (unpaired t test with Welch's correction, p < 0.05) between wild type and mutant alleles are indicated with 'a', from solvent controls with 'b' (means ± SE; n = 4 sets of 15 seedlings each).

(B) Analysis of planar root hair polarity in *act7* and *twd1* in the absence (upper panel) and presence of 1 μM NPA (lower panel). Note apical (shoot-ward) shifts in *act7-4* and *twd1-1* phenocopied by NPA treatments on WT. Color code of root hair positions are indexed from 0 (bottom) to 1 (top end of epidermal cells).

(C) Mutations in *twd1* and *act7* shift trichome development toward 2-branched trichomes, phenocopying WT treated with NPA. Shown is mean occurrence ± SE of one- (red), di- (beige), tri- (green) and four-branched (blue) trichomes derived from n = 4 independent sets of each 10-15 seedlings; significant differences (unpaired *t*-test with Welch's correction, P<0.05) are indicated with 'a'.

(D) Destabilization and stabilization of actin by latrunculin B and jasplakinolide, respectively, blocks hook formation of etiolated seedlings to a similar degree as NPA. Significant differences (unpaired t test with Welch's correction, p < 0.05) from solvent

31

controls are indicated with 'a', between wild type and mutant alleles with 'b' (means ± SE; n = 4 sets of 20 seedlings each).

Figure 6: *twd1* and *act7* show overlapping defects in polar auxin transport.

(A-B) Root auxin responses visualized by the auxin-responsive element DR5:GFP are reduced in the *act7-4* and *twd1-1* columella (**B** quantification of **A**). Bar, 20 μm.

(C) Free IAA is elevated in *act7-4* and *twd1-1* roots.

(D-E) Influx profiles (**D**) and heat map presentation (**E**) of IAA influx along drug-treated (5 μM) WT and *act7-4* roots. Positive fluxes represent a net IAA influx. Significant differences (unpaired *t* test with Welch's correction, $p < 0.05$) from WT solvent controls are indicated by 'a' (mean ± SE; n = 4 sets of 20 (**A-C**) and 12 (**D-E**) seedling each.

Figure 7: Expression of TWD1 alters yeast budding and actin polarity and confers NPA sensitivity.

(A) Confocal images of WT yeast expressing TWD1 in the absence and presence of NPA (10 μM). Actin cables were stained in fixed yeast cells using phalloidin-Alexa Fluor488. scale bar, 5 μm.

(B) Bud size (unpolarized, small-to-medium buds, large buds) of WT yeast expressing TWD1 in the absence and presence of NPA (10 μM). Note NPA resistance of TWD1[K79I] and TWD1[Q82A] shown to not bind NPA (Supplemental Figure 4).

(C) Expression of TWD1 and TWD1[K79I] alters actin polarization, which is reverted by NPA in WT but not in TWD1[K79I]. Significant differences (unpaired *t* test with Welch's correction, $p < 0.05$) between WT and mutant alleles are indicated by 'a', significant differences from solvent controls by 'b' (mean ± SE; n = $\geq$ 3 independent transformants).

TABLES

compound	k_a (1/ M * s)	k_d (1/ s)	K_D (μM)	$\Delta G°$ (kJ/ mol)
NPA	1480 ± 238	0.155 ± 0.013	105 ± 12 (kin) 133 ± 20 (eq)	-22.70 ± 0.28 (kin) -22.14 ± 0.40 (eq)
BUM	645 ± 35	0.175 ± 0.018	272 ± 28 (kin) 252 ± 39 (eq)	-20.36 ± 0.25 (kin) -20.56 ± 0.37 (eq)

TIBA	290 ± 29	0.128 ± 0.007	442 ± 27 (kin) 449 ± 34 (eq)	-19.15 ± 0.16 (kin) -19.10 ± 0.19 (eq)
BA*	543 ± 501	14.318 ± 12.270	33097 ± 11077 (kin) $1.4 \times 10^{19} \pm 4.4 \times 10^{18}$ (eq)	-8.55 ± 0.87 (kin) 75.00 ± 0.73 (eq)

Table 1: Kinetic parameters deduced from surface plasmon resonance (SPR) analyses using TWD1[1-339]. Double referencing and data analysis was performed using Scrubber2 (BioLoglic Software Pty Ltd, Campbell, Australia) and TraceDrawer (Ridgeview Instruments, Vänge, Sweden) analysis software. Affinity binding constants (K_D) were obtained by equilibrium analysis ($K_{D(eq)}$) and by least-squares non-linear fit of the obtained sensograms using a 1:1 Langmuir binding model ($K_{D(kin)}$), which additionally allowed for the evaluation of dissociation (k_d) and association (k_a) rate constants. Values represent means and standard deviations of kinetic constants obtained from at least 3 experiments on independent sensor chips. Corresponding sensograms and fit models are shown in Supplementary Figure 5. *, note that sensograms obtained for BA did not allow for a meaningful fit indicating that TWD[1-339] did not bind BA.

Parameter	WT		twd1-1	
	- NPA [a]	+ NPA [b]	- NPA [c]	+ NPA [d]
Max. filament lifetime (s)	31.1 ± 7.4	47.0 ± 15.7 **	45.1 ± 10.3 *	44.3 ± 11.3
Max. filament length (µm)	27.9 ± 9.9	33.2 ± 14.5 **	28.2 ± 10	28.5 ± 9.1
Elongation rate (µm/s)	2.9 ± 1.0	3.4 ± 1.3 **	2.9 ± 0.9	3.0 ± 1.0
Depolymerization rate (µm/s)	1.4 ± 0.7	1.1 ± 0.8	0.9 * ± 0.4	0.9 ± 0.3
Severing frequency (breaks/ µm/ s)	0.011 ± 0.004	0.008 ± 0.003 **	0.009 * ± 0.003	0.008 ± 0.003
Bundling frequency (events/ µm²/ s)	1.640×10^{-4} $\pm 1.324 \times 10^{-6}$	0.883×10^{-4} $\pm 0.645 \times 10^{-6}$ **	1.890×10^{-4} $\pm 1.314 \times 10^{-6}$	0.872×10^{-4} $\pm 0.999 \times 10^{-6}$ **
Debundling frequency (events/ µm²/ s)	0.590×10^{-4} $\pm 0.2445 \times 10^{-5}$	0.280×10^{-4} $\pm 0.194 \times 10^{-5}$ **	1.910×10^{-4} $\pm 0.414 \times 10^{-5}$ *	0.910×10^{-4} $\pm 0.264 \times 10^{-5}$ **

Table 2: Parameters of actin dynamics deduced from time-lapse variable angle epifluorescence micrososcopy (VAEM) analyses of single, cortical actin filaments of Arabidopsis hypocotyls expressing fABD2-GFP. Shown are means +/- SE of 127 filaments from 34 cells [a], 99 filaments from 31 cells [b], 96 filaments from 41 cells [c], 96 filaments from 46 cells [d]. Significant differences (unpaired *t* test with Welch's correction; p value < 0.01) to WT or solvent controls are indicated by * and **, respectively.

REFERENCES

Abas, L., Benjamins, R., Malenica, N., Paciorek, T., Wisniewska, J., Moulinier-Anzola, J.C., Sieberer, T., Friml, J., and Luschnig, C. (2006). Intracellular trafficking and proteolysis of the Arabidopsis auxin-efflux facilitator PIN2 are involved in root gravitropism. Nat Cell Biol **8,** 249-256.

Bailly, A., Yang, H., Martinoia, E., Geisler, M., and Murphy, A.S. (2012). Plant Lessons: Exploring ABCB Functionality Through Structural Modeling. Frontiers in plant science **2,** 108.

Bailly, A., Sovero, V., Vincenzetti, V., Santelia, D., Bartnik, D., Koenig, B.W., Mancuso, S., Martinoia, E., and Geisler, M. (2008). Modulation of P-glycoproteins by auxin transport inhibitors is mediated by interaction with immunophilins. The Journal of biological chemistry **283,** 21817-21826.

Bailly, A., Wang, B., Zwiewka, M., Pollmann, S., Schenck, D., Luthen, H., Schulz, A., Friml, J., and Geisler, M. (2014). Expression of TWISTED DWARF1 lacking its in-plane membrane anchor leads to increased cell elongation and hypermorphic growth. The Plant journal : for cell and molecular biology **77,** 108-118.

Banasavadi-Siddegowda, Y.K., Mai, J., Fan, Y., Bhattacharya, S., Giovannucci, D.R., Sanchez, E.R., Fischer, G., and Wang, X. (2011). FKBP38 peptidylprolyl isomerase promotes the folding of cystic fibrosis transmembrane conductance regulator in the endoplasmic reticulum. The Journal of biological chemistry **286,** 43071-43080.

Blancaflor, E.B., Wang, Y.S., and Motes, C.M. (2006). Organization and function of the actin cytoskeleton in developing root cells. International review of cytology **252,** 219-264.

Blilou, I., Xu, J., Wildwater, M., Willemsen, V., Paponov, I., Friml, J., Heidstra, R., Aida, M., Palme, K., and Scheres, B. (2005). The PIN auxin efflux facilitator network controls growth and patterning in Arabidopsis roots. Nature **433,** 39-44.

Bouchard, R., Bailly, A., Blakeslee, J.J., Oehring, S.C., Vincenzetti, V., Lee, O.R., Paponov, I., Palme, K., Mancuso, S., Murphy, A.S., Schulz, B., and Geisler, M. (2006). Immunophilin-like TWISTED DWARF1 modulates auxin efflux activities of Arabidopsis P-glycoproteins. The Journal of biological chemistry **281,** 30603-30612.

Burgardt, N.I., Linnert, M., Weiwad, M., Geisler, M., and Lucke, C. (2012). NMR assignments of the FKBP-type PPIase domain of FKBP42 from Arabidopsis thaliana. Biomolecular NMR assignments **6,** 185-188.

Butler, J.H., Hu, S., Brady, S.R., Dixon, M.W., and Muday, G.K. (1998). In vitro and in vivo evidence for actin association of the naphthylphthalamic acid-binding protein from zucchini hypocotyls. The Plant journal : for cell and molecular biology **13,** 291-301.

Casamayor, A., and Snyder, M. (2002). Bud-site selection and cell polarity in budding yeast. Current opinion in microbiology **5,** 179-186.

Cho, M., Lee, S.H., and Cho, H.T. (2007). P-glycoprotein4 displays auxin efflux transporter-like action in Arabidopsis root hair cells and tobacco cells. The Plant cell **19,** 3930-3943.

Cho, M., Lee, Z.W., and Cho, H.T. (2012). ATP-binding cassette B4, an auxin-efflux transporter, stably associates with the plasma membrane and shows distinctive intracellular trafficking from that of PIN-FORMED proteins. Plant physiology **159,** 642-654.

Cox, D.N., and Muday, G.K. (1994). NPA binding activity is peripheral to the plasma membrane and is associated with the cytoskeleton. The Plant cell **6,** 1941-1953.

Dhonukshe, P., Grigoriev, I., Fischer, R., Tominaga, M., Robinson, D.G., Hasek, J., Paciorek, T., Petrasek, J., Seifertova, D., Tejos, R., Meisel, L.A., Zazimalova, E., Gadella, T.W., Jr., Stierhof, Y.D., Ueda, T., Oiwa, K., Akhmanova, A., Brock, R., Spang, A., and Friml, J. (2008). Auxin transport inhibitors impair vesicle motility and actin cytoskeleton dynamics in diverse eukaryotes. Proceedings of the National Academy of Sciences of the United States of America **105,** 4489-4494.

Dixon, M.W., Jacobson, J.A., Cady, C.T., and Muday, G.K. (1996). Cytoplasmic Orientation of the Naphthylphthalamic Acid-Binding Protein in Zucchini Plasma Membrane Vesicles. Plant physiology **112,** 421-432.

Fernandez Rico, J., Lopez, R., Ema, I., and Ramirez, G. (2004). Efficiency of the algorithms for the calculation of Slater molecular integrals in polyatomic molecules. Journal of computational chemistry **25,** 1987-1994.

Friml, J., Benkova, E., Mayer, U., Palme, K., and Muster, G. (2003). Automated whole mount localisation techniques for plant seedlings. The Plant journal : for cell and molecular biology **34,** 115-124.

Geisler, M., and Murphy, A.S. (2006). The ABC of auxin transport: the role of p-glycoproteins in plant development. FEBS letters **580,** 1094-1102.

Geisler, M., Wang, B., and Zhu, J. (2014). Auxin transport during root gravitropism: transporters and techniques. Plant biology **16 Suppl 1,** 50-57.

Geisler, M., Bailly, A., and Ivanchenko, M.G. (2016). Master and servant: Regulation of auxin transporters by FKBPs and cyclophilins. Journal of Plant Science **(in press: 10.1016/j.plantsci.2015.12.004)**.

Geisler, M., Girin, M., Brandt, S., Vincenzetti, V., Plaza, S., Paris, N., Kobae, Y.,

Maeshima, M., Billion, K., Kolukisaoglu, U.H., Schulz, B., and Martinoia, E. (2004). Arabidopsis immunophilin-like TWD1 functionally interacts with vacuolar ABC transporters. Molecular biology of the cell **15,** 3393-3405.

Geisler, M., Kolukisaoglu, H.U., Bouchard, R., Billion, K., Berger, J., Saal, B., Frangne, N., Koncz-Kalman, Z., Koncz, C., Dudler, R., Blakeslee, J.J., Murphy, A.S., Martinoia, E., and Schulz, B. (2003). TWISTED DWARF1, a unique plasma membrane-anchored immunophilin-like protein, interacts with Arabidopsis multidrug resistance-like transporters AtPGP1 and AtPGP19. Molecular biology of the cell **14,** 4238-4249.

Geldner, N., Friml, J., Stierhof, Y.D., Jurgens, G., and Palme, K. (2001). Auxin transport inhibitors block PIN1 cycling and vesicle trafficking. Nature **413,** 425-428.

Gil, P., Dewey, E., Friml, J., Zhao, Y., Snowden, K.C., Putterill, J., Palme, K., Estelle, M., and Chory, J. (2001). BIG: a calossin-like protein required for polar auxin transport in Arabidopsis. Genes Dev **15,** 1985-1997.

Gilliland, L.U., Pawloski, L.C., Kandasamy, M.K., and Meagher, R.B. (2003). Arabidopsis actin gene ACT7 plays an essential role in germination and root growth. The Plant journal : for cell and molecular biology **33,** 319-328.

Granzin, J., Eckhoff, A., and Weiergraber, O.H. (2006). Crystal structure of a multi-domain immunophilin from Arabidopsis thaliana: a paradigm for regulation of plant ABC transporters. J Mol Biol **364,** 799-809.

Grebe, M. (2004). Ups and downs of tissue and planar polarity in plants. Bioessays **26,** 719-729.

Hemenway, C.S., and Heitman, J. (1996). Immunosuppressant target protein FKBP12 is required for P-glycoprotein function in yeast. The Journal of biological chemistry **271,** 18527-18534.

Henrichs, S., Wang, B., Fukao, Y., Zhu, J., Charrier, L., Bailly, A., Oehring, S.C., Linnert, M., Weiwad, M., Endler, A., Nanni, P., Pollmann, S., Mancuso, S., Schulz, A., and Geisler, M. (2012). Regulation of ABCB1/PGP1-catalysed auxin transport by linker phosphorylation. The EMBO journal **31,** 2965-2980.

Henty, J.L., Bledsoe, S.W., Khurana, P., Meagher, R.B., Day, B., Blanchoin, L., and Staiger, C.J. (2011). Arabidopsis actin depolymerizing factor4 modulates the stochastic dynamic behavior of actin filaments in the cortical array of epidermal cells. The Plant cell **23,** 3711-3726.

Henty-Ridilla, J.L., Li, J., Blanchoin, L., and Staiger, C.J. (2013). Actin dynamics in the cortical array of plant cells. Current opinion in plant biology **16,** 678-687.

Higaki, T., Kutsuna, N., Sano, T., Kondo, N., and Hasezawa, S. (2010). Quantification and cluster analysis of actin cytoskeletal structures in plant cells: role of actin bundling in stomatal movement during diurnal cycles in Arabidopsis guard cells. The Plant journal : for cell and molecular biology **61,** 156-165.

Hoffmann, C., Moreau, F., Moes, M., Luthold, C., Dieterle, M., Goretti, E., Neumann, K., Steinmetz, A., and Thomas, C. (2014a). Human muscle LIM protein dimerizes along the actin cytoskeleton and cross-links actin filaments. Molecular and cellular

biology **34,** 3053-3065.

Hoffmann, C., Moes, D., Dieterle, M., Neumann, K., Moreau, F., Tavares Furtado, A., Dumas, D., Steinmetz, A., and Thomas, C. (2014b). Live cell imaging reveals actin-cytoskeleton-induced self-association of the actin-bundling protein WLIM1. Journal of cell science **127,** 583-598.

Holweg, C., and Nick, P. (2004). Arabidopsis myosin XI mutant is defective in organelle movement and polar auxin transport. Proceedings of the National Academy of Sciences of the United States of America **101,** 10488-10493.

Holweg, C., Susslin, C., and Nick, P. (2004). Capturing in vivo dynamics of the actin cytoskeleton stimulated by auxin or light. Plant & cell physiology **45,** 855-863.

Jacobs, M., and Rubery, P.H. (1988). Naturally-Occurring Auxin Transport Regulators. Science **241,** 346-349.

Kamphausen, T., Fanghanel, J., Neumann, D., Schulz, B., and Rahfeld, J.U. (2002). Characterization of Arabidopsis thaliana AtFKBP42 that is membrane-bound and interacts with Hsp90. The Plant journal : for cell and molecular biology **32,** 263-276.

Kandasamy, M.K., McKinney, E.C., and Meagher, R.B. (2009). A single vegetative actin isovariant overexpressed under the control of multiple regulatory sequences is sufficient for normal Arabidopsis development. The Plant cell **21,** 701-718.

Kandasamy, M.K., Gilliland, L.U., McKinney, E.C., and Meagher, R.B. (2001). One plant actin isovariant, ACT7, is induced by auxin and required for normal callus formation. The Plant cell **13,** 1541-1554.

Kania, U., Fendrych, M., and Friml, J. (2014). Polar delivery in plants; commonalities and differences to animal epithelial cells. Open biology **4,** 140017.

Kiefer, C.S., Claes, A.R., Nzayisenga, J.C., Pietra, S., Stanislas, T., Huser, A., Ikeda, Y., and Grebe, M. (2015). Arabidopsis AIP1-2 restricted by WER-mediated patterning modulates planar polarity. Development **142,** 151-161.

Kim, J.Y., Henrichs, S., Bailly, A., Vincenzetti, V., Sovero, V., Mancuso, S., Pollmann, S., Kim, D., Geisler, M., and Nam, H.G. (2010). Identification of an ABCB/P-glycoprotein-specific inhibitor of auxin transport by chemical genomics. The Journal of biological chemistry **285,** 23309-23317.

Kleine-Vehn, J., and Friml, J. (2008). Polar targeting and endocytic recycling in auxin-dependent plant development. Annual review of cell and developmental biology **24,** 447-473.

Kleine-Vehn, J., Dhonukshe, P., Swarup, R., Bennett, M., and Friml, J. (2006). Subcellular trafficking of the Arabidopsis auxin influx carrier AUX1 uses a novel pathway distinct from PIN1. The Plant cell **18,** 3171-3181.

Kubes, M., Yang, H., Richter, G.L., Cheng, Y., Mlodzinska, E., Wang, X., Blakeslee, J.J., Carraro, N., Petrasek, J., Zazimalova, E., Hoyerova, K., Peer, W.A., and Murphy, A.S. (2012). The Arabidopsis concentration-dependent influx/efflux transporter ABCB4 regulates cellular auxin levels in the root epidermis. The Plant journal : for cell and molecular biology **69,** 640-654.

Lanza, M., Garcia-Ponce, B., Castrillo, G., Catarecha, P., Sauer, M., Rodriguez-Serrano, M., Paez-Garcia, A., Sanchez-Bermejo, E., T, C.M., Leo del Puerto, Y., Sandalio, L.M., Paz-Ares, J., and Leyva, A. (2012). Role of actin cytoskeleton in brassinosteroid signaling and in its integration with the auxin response in plants. Developmental cell **22,** 1275-1285.

Li, G., Liang, W., Zhang, X., Ren, H., Hu, J., Bennett, M.J., and Zhang, D. (2014). Rice actin-binding protein RMD is a key link in the auxin-actin regulatory loop that controls cell growth. Proceedings of the National Academy of Sciences of the United States of America **111,** 10377-10382.

Luschnig, C. (2001). Auxin transport: why plants like to think BIG. Current biology : CB **11,** R831-833.

Luschnig, C. (2002). Auxin transport: ABC proteins join the club. Trends in plant science **7,** 329-332.

Mancuso, S., Marras, A.M., Magnus, V., and Baluska, F. (2005). Noninvasive and continuous recordings of auxin fluxes in intact root apex with a carbon nanotube-modified and self-referencing microelectrode. Anal Biochem **341,** 344-351.

Masucci, J.D., and Schiefelbein, J.W. (1994). The rhd6 Mutation of Arabidopsis thaliana Alters Root-Hair Initiation through an Auxin- and Ethylene-Associated Process. Plant physiology **106,** 1335-1346.

Muday, G.K. (2000). Maintenance of asymmetric cellular localization of an auxin transport protein through interaction with the actin cytoskeleton. Journal of plant growth regulation **19,** 385-396.

Muday, G.K., and Murphy, A.S. (2002). An emerging model of auxin transport regulation. The Plant cell **14,** 293-299.

Murphy, A.S., Hoogner, K.R., Peer, W.A., and Taiz, L. (2002). Identification, purification, and molecular cloning of N-1-naphthylphthalmic acid-binding plasma membrane-associated aminopeptidases from Arabidopsis. Plant physiology **128,** 935-950.

Mussar, K.J., Kandasamy, M.K., McKinney, E.C., and Meagher, R.B. (2015). Arabidopsis plants deficient in constitutive class profilins reveal independent and quantitative genetic effects. BMC plant biology **15,** 177.

Nagashima, A., Suzuki, G., Uehara, Y., Saji, K., Furukawa, T., Koshiba, T., Sekimoto, M., Fujioka, S., Kuroha, T., Kojima, M., Sakakibara, H., Fujisawa, N., Okada, K., and Sakai, T. (2008). Phytochromes and cryptochromes regulate the differential growth of Arabidopsis hypocotyls in both a PGP19-dependent and a PGP19-independent manner. The Plant journal : for cell and molecular biology **53,** 516-529.

Nick, P., Han, M.J., and An, G. (2009). Auxin stimulates its own transport by shaping actin filaments. Plant physiology **151,** 155-167.

Okada, K., Ueda, J., Komaki, M.K., Bell, C.J., and Shimura, Y. (1991). Requirement of the Auxin Polar Transport System in Early Stages of Arabidopsis Floral Bud Formation. The Plant cell **3,** 677-684.

Ottenschlager, I., Wolff, P., Wolverton, C., Bhalerao, R.P., Sandberg, G., Ishikawa, H.,

Evans, M., and Palme, K. (2003). Gravity-regulated differential auxin transport from columella to lateral root cap cells. Proceedings of the National Academy of Sciences of the United States of America **100,** 2987-2991.

Paciorek, T., Zazimalova, E., Ruthardt, N., Petrasek, J., Stierhof, Y.D., Kleine-Vehn, J., Morris, D.A., Emans, N., Jurgens, G., Geldner, N., and Friml, J. (2005). Auxin inhibits endocytosis and promotes its own efflux from cells. Nature **435,** 1251-1256.

Papuga, J., Hoffmann, C., Dieterle, M., Moes, D., Moreau, F., Tholl, S., Steinmetz, A., and Thomas, C. (2010). Arabidopsis LIM proteins: a family of actin bundlers with distinct expression patterns and modes of regulation. The Plant cell **22,** 3034-3052.

Peer, W.A., and Murphy, A.S. (2007). Flavonoids and auxin transport: modulators or regulators? Trends in plant science **12,** 556-563.

Peer, W.A., Hosein, F.N., Bandyopadhyay, A., Makam, S.N., Otegui, M.S., Lee, G.J., Blakeslee, J.J., Cheng, Y., Titapiwatanakun, B., Yakubov, B., Bangari, B., and Murphy, A.S. (2009). Mutation of the membrane-associated M1 protease APM1 results in distinct embryonic and seedling developmental defects in Arabidopsis. The Plant cell **21,** 1693-1721.

Petrasek, J., Cerna, A., Schwarzerova, K., Elckner, M., Morris, D.A., and Zazimalova, E. (2003). Do phytotropins inhibit auxin efflux by impairing vesicle traffic? Plant physiology **131,** 254-263.

Petrasek, J., Mravec, J., Bouchard, R., Blakeslee, J.J., Abas, M., Seifertova, D., Wisniewska, J., Tadele, Z., Kubes, M., Covanova, M., Dhonukshe, P., Skupa, P., Benkova, E., Perry, L., Krecek, P., Lee, O.R., Fink, G.R., Geisler, M., Murphy, A.S., Luschnig, C., Zazimalova, E., and Friml, J. (2006). PIN proteins perform a rate-limiting function in cellular auxin efflux. Science **312,** 914-918.

Rahman, A., Bannigan, A., Sulaman, W., Pechter, P., Blancaflor, E.B., and Baskin, T.I. (2007). Auxin, actin and growth of the Arabidopsis thaliana primary root. The Plant journal : for cell and molecular biology **50,** 514-528.

Rojas-Pierce, M., Titapiwatanakun, B., Sohn, E.J., Fang, F., Larive, C.K., Blakeslee, J., Cheng, Y., Cutler, S.R., Peer, W.A., Murphy, A.S., and Raikhel, N.V. (2007). Arabidopsis P-glycoprotein19 participates in the inhibition of gravitropism by gravacin. Chem Biol **14,** 1366-1376.

Scheidt, H.A., Vogel, A., Eckhoff, A., Koenig, B.W., and Huster, D. (2006). Solid-state NMR characterization of the putative membrane anchor of TWD1 from Arabidopsis thaliana. Eur Biophys J.

Schenck, D., Christian, M., Jones, A., and Luthen, H. (2010). Rapid auxin-induced cell expansion and gene expression: a four-decade-old question revisited. Plant physiology **152,** 1183-1185.

Seeliger, D., and de Groot, B.L. (2010). Ligand docking and binding site analysis with PyMOL and Autodock/Vina. Journal of computer-aided molecular design **24,** 417-422.

Sheahan, M.B., Staiger, C.J., Rose, R.J., and McCurdy, D.W. (2004). A green fluorescent protein fusion to actin-binding domain 2 of Arabidopsis fimbrin highlights

new features of a dynamic actin cytoskeleton in live plant cells. Plant physiology **136,** 3968-3978.

Staiger, C.J., Sheahan, M.B., Khurana, P., Wang, X., McCurdy, D.W., and Blanchoin, L. (2009). Actin filament dynamics are dominated by rapid growth and severing activity in the Arabidopsis cortical array. The Journal of cell biology **184,** 269-280.

Szymanski, W.G., Zauber, H., Erban, A., Gorka, M., Wu, X.N., and Schulze, W.X. (2015). Cytoskeletal Components Define Protein Location to Membrane Microdomains. Molecular & cellular proteomics : MCP **14,** 2493-2509.

Thomas, C. (2012). Bundling actin filaments from membranes: some novel players. Frontiers in plant science **3,** 188.

Titapiwatanakun, B., Blakeslee, J.J., Bandyopadhyay, A., Yang, H., Mravec, J., Sauer, M., Cheng, Y., Adamec, J., Nagashima, A., Geisler, M., Sakai, T., Friml, J., Peer, W.A., and Murphy, A.S. (2009). ABCB19/PGP19 stabilises PIN1 in membrane microdomains in Arabidopsis. The Plant journal : for cell and molecular biology **57,** 27-44.

van der Honing, H.S., Kieft, H., Emons, A.M., and Ketelaar, T. (2012). Arabidopsis VILLIN2 and VILLIN3 are required for the generation of thick actin filament bundles and for directional organ growth. Plant physiology **158,** 1426-1438.

Vanneste, S., and Friml, J. (2009). Auxin: a trigger for change in plant development. Cell **136,** 1005-1016.

Wang, B., Bailly, A., Zwiewka, M., Henrichs, S., Azzarello, E., Mancuso, S., Maeshima, M., Friml, J., Schulz, A., and Geisler, M. (2013). Arabidopsis TWISTED DWARF1 functionally interacts with auxin exporter ABCB1 on the root plasma membrane. The Plant cell **25,** 202-214.

Weiergraber, O.H., Eckhoff, A., and Granzin, J. (2006). Crystal structure of a plant immunophilin domain involved in regulation of MDR-type ABC transporters. FEBS letters **580,** 251-255.

Wu, G., Otegui, M.S., and Spalding, E.P. (2010). The ER-localized TWD1 immunophilin is necessary for localization of multidrug resistance-like proteins required for polar auxin transport in Arabidopsis roots. The Plant cell **22,** 3295-3304.

Wu, S., Xie, Y., Zhang, J., Ren, Y., Zhang, X., Wang, J., Guo, X., Wu, F., Sheng, P., Wang, J., Wu, C., Wang, H., Huang, S., and Wan, J. (2015). VLN2 Regulates Plant Architecture by Affecting Microfilament Dynamics and Polar Auxin Transport in Rice. The Plant cell **27,** 2829-2845.

Yu, J.H., Crevenna, A.H., Bettenbuhl, M., Freisinger, T., and Wedlich-Soldner, R. (2011). Cortical actin dynamics driven by formins and myosin V. Journal of cell science **124,** 1533-1541.

Zadnikova, P., Petrasek, J., Marhavy, P., Raz, V., Vandenbussche, F., Ding, Z., Schwarzerova, K., Morita, M.T., Tasaka, M., Hejatko, J., Van Der Straeten, D., Friml, J., and Benkova, E. (2010). Role of PIN-mediated auxin efflux in apical hook development of Arabidopsis thaliana. Development **137,** 607-617.

1424   **Zhu, J., and Geisler, M.** (2015b). Keeping it all together: auxin-actin crosstalk in plant
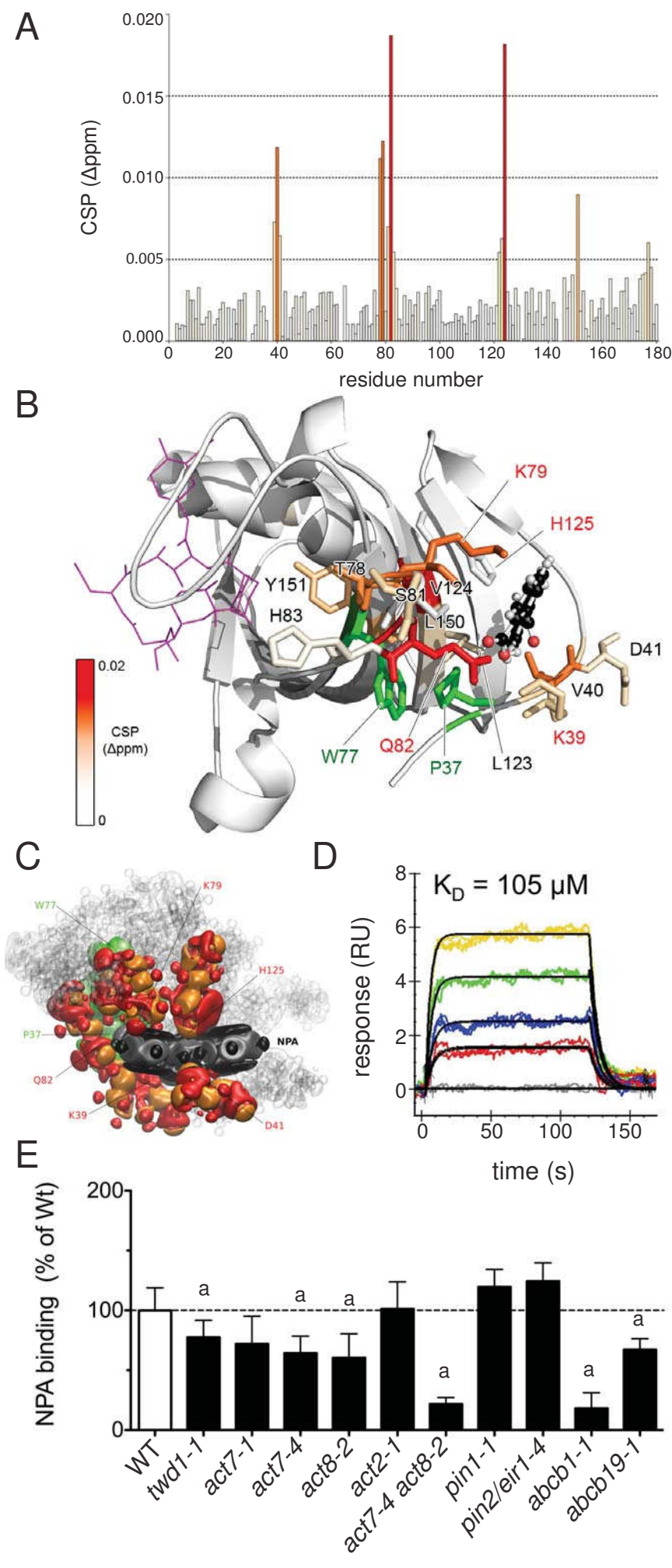1425   development. Journal of experimental botany **66,** 4983-4998.

Figure 1: TWISTED DWARF1 (TWD1) is a low-affinity NPA binding protein (A) NMR chemical shift perturbation (CSP) analysis of NPA binding to TWD11-180 revealing combined 1H and 15N chemical shift changes. Relevant residues for the binding of NPA above 0.005 ppm are colored according to the legend in (B). (B) Most stable quantum chemical modeling-derived NPA-bound conformations (balls and sticks) correlate with the mapping of CSP values on FKBP4234-180 (PDB ID 2IF4, color code reflects CSP shifts). Side chains of residues assumed to participate in the binding surface are depicted as sticks; relevant TWD1 mutations are in red. Theoretical FK506-binding to the non-canonical PPIase domain (PDB 1FKJ) is indicated in magenta; W77 and P37 thought to build a stacking interaction are colored in green. (C) Quantum chemical analysis of the electron density components responsible for the Van der Waals forces between NPA and the surrounding amino acids. Electronic density deformation for NPA (dipole-type deformation in grey and quadrupole-type deformation in black) and for the amino acid residues (dipole-type deformation in orange and quadrupole-type deformation in red; see also Supplemental Figure 3). (D) Kinetic analysis of NPA binding to thiol-immobilized TWD11-339. Sensograms of injections of 15 μM, 30 μM, 60 μM and 90 μM NPA in color and representative kinetic fit models (1:1) indicated in black. Data is representative for 3 independent experiments with comparable results (see Table 1). Residuals and goodness-of-fit are indicated in Supplemental Figure 5. (E) Specific 3H-NPA binding calculated as difference between total and unspecific NPA binding determined in the absence (total) and presence of a 1000-fold access of non-radiolabelled NPA concentrations (unspecific). Significant differences (unpaired t-test with Welch's correction, P<0.05) from corresponding WS and Col-0 wild types (WT), respectively, are indicated by 'a'.

Figure 2: Actin architecture and NPA sensitivity is altered in twd1. (A-C) Time-lapse variable angle epifluorescence microscopy (VAEM) analyses of cortical actin of dark-grown hypocotyl expressing fABD2-GFP treated with 1 μM NPA. Representative epidermal cells (A) and quantification of actin bundling (skewness, B) and percent occupancy (density, C); bar, 10 μm. Significant differences (unpaired t test with Welch's correction, $p < 0.05$) between wild type (WT) and mutant alleles are indicated by 'a', significant differences to solvent controls by 'b' (mean ± SE; n ≥ 100).

Figure 3: ACT7 regulates ABCB and PIN-type auxin transporter and TWD1 expression and location. (A-B) Auxin transporters, ABCB1,4,19-GFP (A) and PIN1,2-GFP, as well as the ABCB chaperon, TWD1-CFP (B), are delocalized from the root PM and ER, respectively, and retained on punctuated structures (arrows) and are significantly down-regulated in act7-4 in comparison to the corresponding WT lines. Bars, 10 μm.

(C) Quantification of (A-B). Significant differences (unpaired t test with Welch's correction, $p < 0.05$) between wild type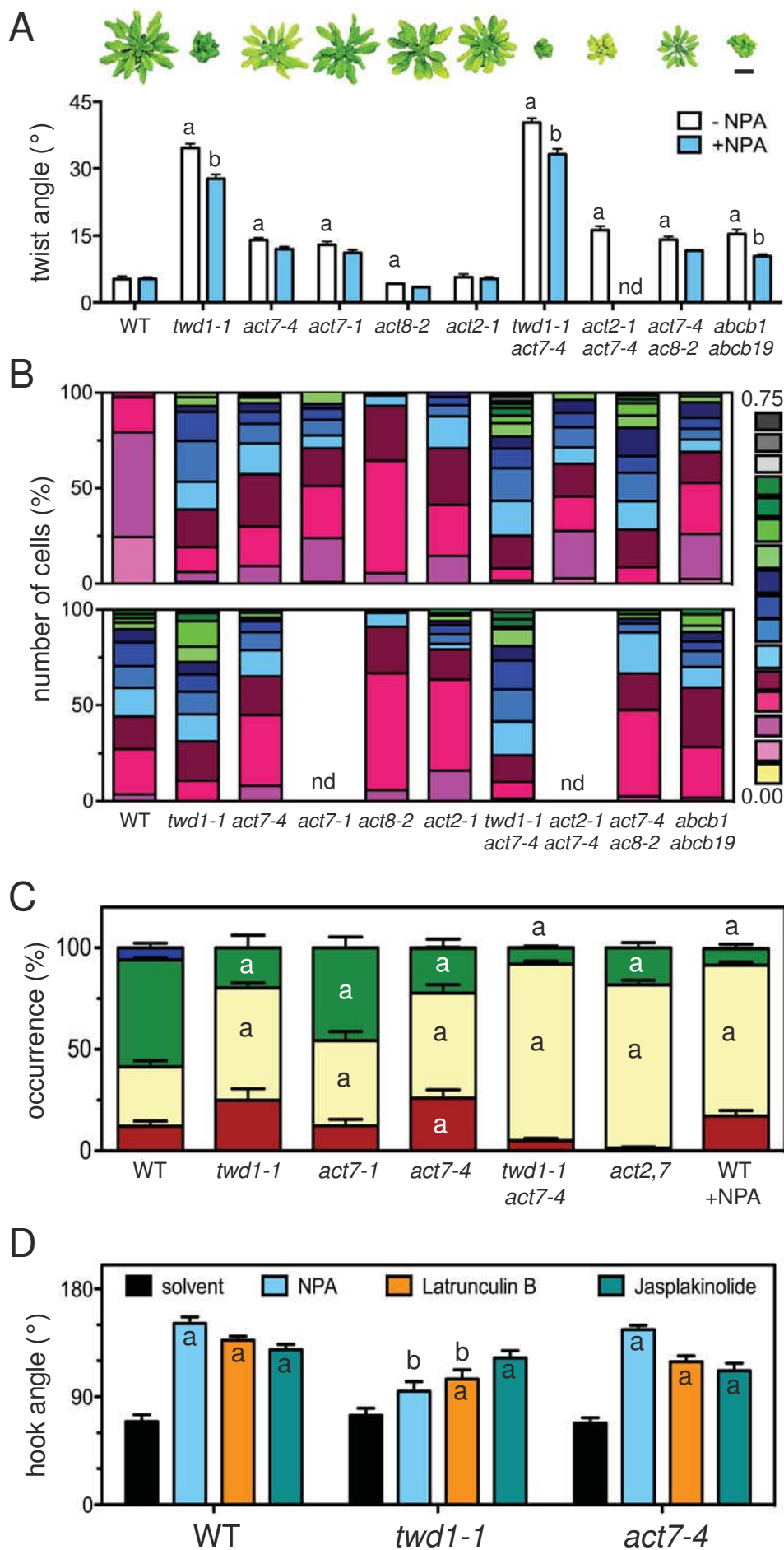 and act7-4 are indicated by 'a' (mean ± SE; n ≥ 50 images). Note that GFP quantifications by confocal imaging were performed over identically defined areas of the entire root tip and therefore quantified intensities in (C) might not match pictures in (A-B). Further, that for PIN1,2-GFP and ABCB4-GFP non-isogenic lines were used for analyses in act7-4 but that artifacts caused by ecotype mixes were excluded by immunolocalizations or isogenic controls (Supplemental Figure 13).

Figure 4: ABCB and PIN-type auxin exporters co-localize with vacuolar markers in act7-4. (A) ABCB4-GFP, ABCB19-GFP, PIN1-GFP and PIN2-GFP co-localize (arrows) with compartments stained after long FM4-64 treatments (4 µM, 3 h) in act7-4 indicating vacuolar origin. (C) ABCB19 and PIN1, and to a lesser extent ABCB4 and PIN2, co-localize with late vacuolar marker, lysotracker red (LTR), in act7-4. Bars, 10 µm. (B, D) Quantification of ABCB and PIN co-localization in WT and act7-4 with FM4-64 (B) and LTR markers (D). Significant differences (unpaired t test with Welch's correction, $p < 0.05$) between wild type and act7-4 are indicated by 'a' (mean ± SE; n ≥ 50 images).

Figure 5: twd1 and act7 show overlapping developmental phenotypes

(A) act7-4 like twd1-1 shows a reduction in growth (upper panel; scale bar, 2 cm) and a significant disorientation of epidermal layers to the growth direction (twist angle, lower panel). Significant differences (unpaired t test with Welch's correction, $p < 0.05$) between wild type and mutant alleles are indicated with 'a', from solvent controls with 'b' (means ± SE; n = 4 sets of 15 seedlings each).
(B) Analysis of planar root hair polarity in act7 and twd1 in the absence (upper panel) and presence of 1 µM NPA (lower panel). Note apical (shoot-ward) shifts in act7-4 and twd1-1 phenocopied by NPA treatments on WT. Color code of root hair positions are indexed from 0 (bottom) to 1 (top end of epidermal cells).
(C) Mutations in twd1 and act7 shift trichome development toward 2-branched trichomes, phenocopying WT treated with NPA. Shown is mean occurrence ± SE of one- (red), di- (beige), tri- (green) and four-branched (blue) trichomes derived from n = 4 independent sets of each 10-15 seedlings; significant differences (unpaired t-test with Welch's correction, P<0.05) are indicated with 'a'.
(D) Destabilization and stabilization of actin by latrunculin B and jasplakinolide, respectively, blocks hook formation of etiolated seedlings to a similar degree as NPA. Significant differences (unpaired t test with Welch's correction, $p < 0.05$) from solvent controls are indicated with 'a', between wild type and mutant alleles with 'b' (means ± SE; n = 4 sets of 20 seedlings each).
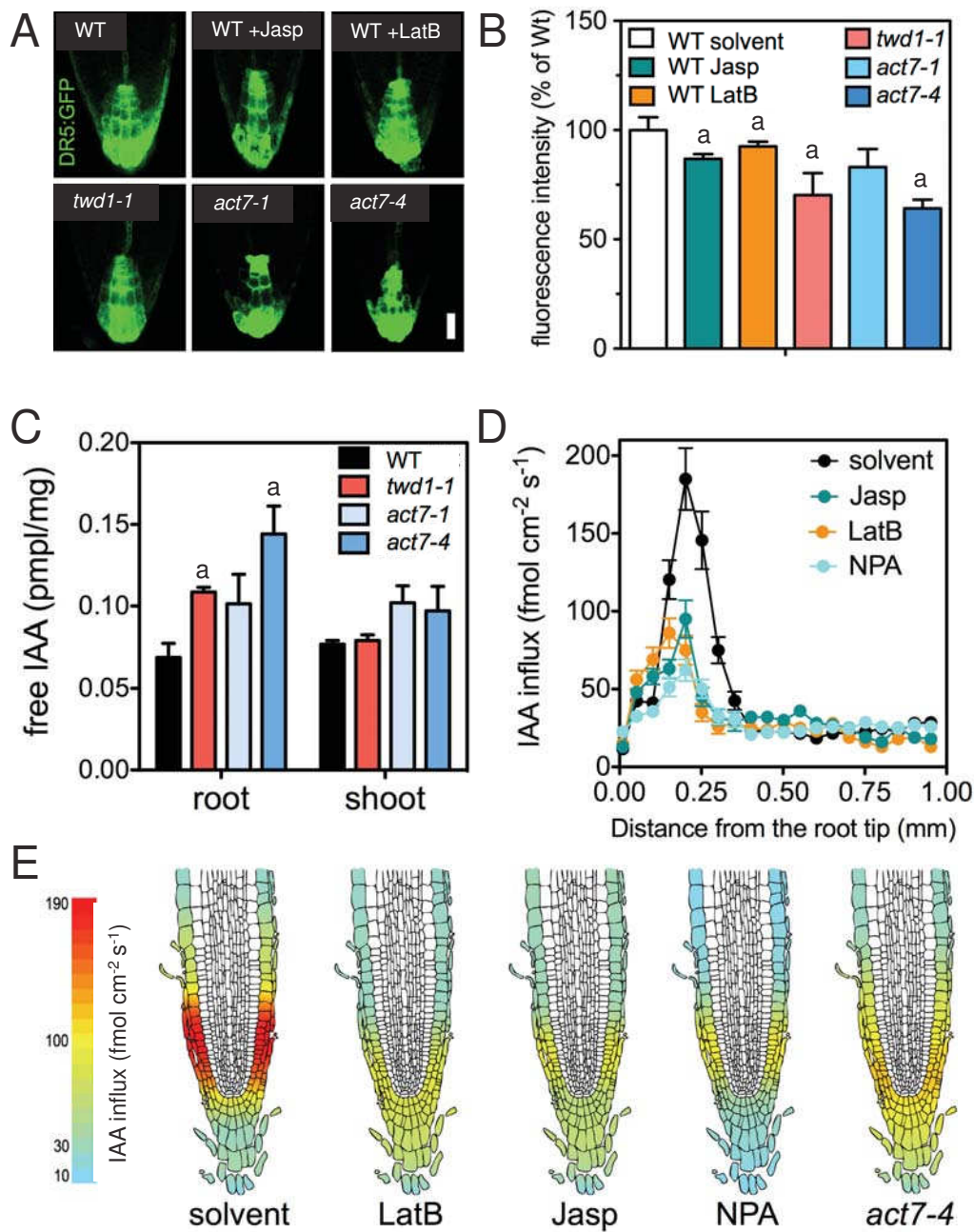
Figure 6: twd1 and act7 show overlapping defects in polar auxin transport. (A-B) Root auxin responses visualized by the auxin-responsive element DR5:GFP are reduced in the act7-4 and twd1-1 columella (B quantification of A). Bar, 20 μm. (C) Free IAA is elevated in act7-4 and twd1-1 roots. (D-E) Influx profiles (D) and heat map presentation (E) of IAA influx along drug-treated (5 μM) WT and act7-4 roots. Positive fluxes represent a net IAA influx. Significant differences (unpaired t test with Welch's correction, $p < 0.05$) from WT solvent controls are indicated by 'a' (mean ± SE; n = 4 sets of 20 (A-C) and 12 (D-E) seedling each.

Figure 7: Expression of TWD1 alters yeast budding and actin polarity and confers NPA sensitivity. (A) Confocal images of WT yeast expressing TWD1 in the absence and presence of NPA (10 μM). Actin cables were stained in fixed yeast cells using phalloidin-Alexa Fluor488. scale bar, 5 μm. (B) Bud size (unpolarized, small-to-medium buds, large buds) of WT yeast expressing TWD1 in the absence and presence of NPA (10 μM). Note NPA resistance of TWD1K79I and TWD1Q82A shown to not bind NPA (Supplemental Figure 4). (C) Expression of TWD1 and TWD1K79I alters actin polarization, which is reverted by NPA in WT but not in TWD1K79I. Significant differences (unpaired t test with Welch's correction, $p < 0.05$) between WT and mutant alleles are indicated by 'a', significant differences from solvent controls by 'b' (mean ± SE; n = ≥ 3 independent transformants).

Parsed Citations

Abas, L., Benjamins, R., Malenica, N., Paciorek, T., Wisniewska, J., Moulinier-Anzola, J.C., Sieberer, T., Friml, J., and Luschnig, C. (2006). Intracellular trafficking and proteolysis of the Arabidopsis auxin-efflux facilitator PIN2 are involved in root gravitropism. Nat Cell Biol 8, 249-256.
Pubmed: Author and Title
CrossRef: Author and Title
Google Scholar: Author Only Title Only Author and Title

Bailly, A, Yang, H., Martinoia, E., Geisler, M., and Murphy, A.S. (2012). Plant Lessons: Exploring ABCB Functionality Through Structural Modeling. Frontiers in plant science 2, 108.
Pubmed: Author and Title
CrossRef: Author and Title
Google Scholar: Author Only Title Only Author and Title

Bailly, A, Sovero, V., Vincenzetti, V., Santelia, D., Bartnik, D., Koenig, B.W., Mancuso, S., Martinoia, E., and Geisler, M. (2008). Modulation of P-glycoproteins by auxin transport inhibitors is mediated by interaction with immunophilins. The Journal of biological chemistry 283, 21817-21826.
Pubmed: Author and Title
CrossRef: Author and Title
Google Scholar: Author Only Title Only Author and Title

Bailly, A, Wang, B., Zwiewka, M., Pollmann, S., Schenck, D., Luthen, H., Schulz, A, Friml, J., and Geisler, M. (2014). Expression of TWISTED DWARF1 lacking its in-plane membrane anchor leads to increased cell elongation and hypermorphic growth. The Plant journal : for cell and molecular biology 77, 108-118.
Pubmed: Author and Title
CrossRef: Author and Title
Google Scholar: Author Only Title Only Author and Title

Banasavadi-Siddegowda, Y.K., Mai, J., Fan, Y., Bhattacharya, S., Giovannucci, D.R., Sanchez, E.R., Fischer, G., and Wang, X. (2011). FKBP38 peptidylprolyl isomerase promotes the folding of cystic fibrosis transmembrane conductance regulator in the endoplasmic reticulum. The Journal of biological chemistry 286, 43071-43080.
Pubmed: Author and Title
CrossRef: Author and Title
Google Scholar: Author Only Title Only Author and Title

Blancaflor, E.B., Wang, Y.S., and Motes, C.M. (2006). Organization and function of the actin cytoskeleton in developing root cells. International review of cytology 252, 219-264.
Pubmed: Author and Title
CrossRef: Author and Title
Google Scholar: Author Only Title Only Author and Title

Blilou, I., Xu, J., Wildwater, M., Willemsen, V., Paponov, I., Friml, J., Heidstra, R., Aida, M., Palme, K., and Scheres, B. (2005). The PIN auxin efflux facilitator network controls growth and patterning in Arabidopsis roots. Nature 433, 39-44.
Pubmed: Author and Title
CrossRef: Author and Title
Google Scholar: Author Only Title Only Author and Title

Bouchard, R., Bailly, A, Blakeslee, J.J., Oehring, S.C., Vincenzetti, V., Lee, O.R., Paponov, I., Palme, K., Mancuso, S., Murphy, A.S., Schulz, B., and Geisler, M. (2006). Immunophilin-like TWISTED DWARF1 modulates auxin efflux activities of Arabidopsis P-glycoproteins. The Journal of biological chemistry 281, 30603-30612.
Pubmed: Author and Title
CrossRef: Author and Title
Google Scholar: Author Only Title Only Author and Title

Burgardt, N.I., Linnert, M., Weiwad, M., Geisler, M., and Lucke, C. (2012). NMR assignments of the FKBP-type PPIase domain of FKBP42 from Arabidopsis thaliana. Biomolecular NMR assignments 6, 185-188.
Pubmed: Author and Title
CrossRef: Author and Title
Google Scholar: Author Only Title Only Author and Title

Butler, J.H., Hu, S., Brady, S.R., Dixon, M.W., and Muday, G.K. (1998). In vitro and in vivo evidence for actin association of the naphthylphthalamic acid-binding protein from zucchini hypocotyls. The Plant journal : for cell and molecular biology 13, 291-301.
Pubmed: Author and Title
CrossRef: Author and Title
Google Scholar: Author Only Title Only Author and Title

Casamayor, A, and Snyder, M. (2002). Bud-site selection and cell polarity in budding yeast. Current opinion in microbiology 5, 179-186.
Pubmed: Author and Title
CrossRef: Author and Title
Google Scholar: Author Only Title Only Author and Title

Cho, M., Lee, S.H., and Cho, H.T. (2007). P-glycoprotein4 displays auxin efflux transporter-like action in Arabidopsis root hair cells and tobacco cells. The Plant cell 19, 3930-3943.
Pubmed: Author and Title
CrossRef: Author and Title
Google Scholar: Author Only Title Only Author and Title

Cho, M., Lee, Z.W., and Cho, H.T. (2012). ATP-binding cassette B4, an auxin-efflux transporter, stably associates with the plasma membrane and shows distinctive intracellular trafficking from that of PIN-FORMED proteins. Plant physiology 159, 642-654.
Pubmed: Author and Title
CrossRef: Author and Title
Google Scholar: Author Only Title Only Author and Title

Cox, D.N., and Muday, G.K. (1994). NPA binding activity is peripheral to the plasma membrane and is associated with the cytoskeleton. The Plant cell 6, 1941-1953.
Pubmed: Author and Title
CrossRef: Author and Title
Google Scholar: Author Only Title Only Author and Title

Dhonukshe, P., Grigoriev, I., Fischer, R., Tominaga, M., Robinson, D.G., Hasek, J., Paciorek, T., Petrasek, J., Seifertova, D., Tejos, R., Meisel, L.A., Zazimalova, E., Gadella, T.W., Jr., Stierhof, Y.D., Ueda, T., Oiwa, K., Akhmanova, A., Brock, R., Spang, A., and Friml, J. (2008). Auxin transport inhibitors impair vesicle motility and actin cytoskeleton dynamics in diverse eukaryotes. Proceedings of the National Academy of Sciences of the United States of America 105, 4489-4494.
Pubmed: Author and Title
CrossRef: Author and Title
Google Scholar: Author Only Title Only Author and Title

Dixon, M.W., Jacobson, J.A., Cady, C.T., and Muday, G.K. (1996). Cytoplasmic Orientation of the Naphthylphthalamic Acid-Binding Protein in Zucchini Plasma Membrane Vesicles. Plant physiology 112, 421-432.
Pubmed: Author and Title
CrossRef: Author and Title
Google Scholar: Author Only Title Only Author and Title

Fernandez Rico, J., Lopez, R., Ema, I., and Ramirez, G. (2004). Efficiency of the algorithms for the calculation of Slater molecular integrals in polyatomic molecules. Journal of computational chemistry 25, 1987-1994.
Pubmed: Author and Title
CrossRef: Author and Title
Google Scholar: Author Only Title Only Author and Title

Friml, J., Benkova, E., Mayer, U., Palme, K., and Muster, G. (2003). Automated whole mount localisation techniques for plant seedlings. The Plant journal : for cell and molecular biology 34, 115-124.
Pubmed: Author and Title
CrossRef: Author and Title
Google Scholar: Author Only Title Only Author and Title

Geisler, M., and Murphy, A.S. (2006). The ABC of auxin transport: the role of p-glycoproteins in plant development. FEBS letters 580, 1094-1102.
Pubmed: Author and Title
CrossRef: Author and Title
Google Scholar: Author Only Title Only Author and Title

Geisler, M., Wang, B., and Zhu, J. (2014). Auxin transport during root gravitropism: transporters and techniques. Plant biology 16 Suppl 1, 50-57.
Pubmed: Author and Title
CrossRef: Author and Title
Google Scholar: Author Only Title Only Author and Title

Geisler, M., Bailly, A., and Ivanchenko, M.G. (2016). Master and servant: Regulation of auxin transporters by FKBPs and cyclophilins. Journal of Plant Science (in press: 10.1016/j.plantsci.2015.12.004).
Pubmed: Author and Title
CrossRef: Author and Title
Google Scholar: Author Only Title Only Author and Title

Geisler, M., Girin, M., Brandt, S., Vincenzetti, V., Plaza, S., Paris, N., Kobae, Y., Maeshima, M., Billion, K., Kolukisaoglu, U.H., Schulz, B., and Martinoia, E. (2004). Arabidopsis immunophilin-like TWD1 functionally interacts with vacuolar ABC transporters. Molecular biology of the cell 15, 3393-3405.
Pubmed: Author and Title
CrossRef: Author and Title
Google Scholar: Author Only Title Only Author and Title

Geisler, M., Kolukisaoglu, H.U., Bouchard, R., Billion, K., Berger, J., Saal, B., Frangne, N., Koncz-Kalman, Z., Koncz, C., Dudler, R., Blakeslee, J.J., Murphy, A.S., Martinoia, E., and Schulz, B. (2003). TWISTED DWARF1, a unique plasma membrane-anchored immunophilin-like protein, interacts with Arabidopsis multidrug resistance-like transporters AtPGP1 and AtPGP19. Molecular biology of the cell 14, 4238-4249.
Pubmed: Author and Title
CrossRef: Author and Title
Google Scholar: Author Only Title Only Author and Title

Geldner, N., Friml, J., Stierhof, Y.D., Jurgens, G., and Palme, K. (2001). Auxin transport inhibitors block PIN1 cycling and vesicle trafficking. Nature 413, 425-428.
Pubmed: Author and Title
CrossRef: Author and Title
Google Scholar: Author Only Title Only Author and Title

Gil, P., Dewey, E., Friml, J., Zhao, Y., Snowden, K.C., Putterill, J., Palme, K., Estelle, M., and Chory, J. (2001). BIG: a calossin-like protein required for polar auxin transport in Arabidopsis. Genes Dev 15, 1985-1997.
Pubmed: Author and Title

CrossRef: Author and Title
Google Scholar: Author Only Title Only Author and Title

Gilliland, L.U., Pawloski, L.C., Kandasamy, M.K., and Meagher, R.B. (2003). Arabidopsis actin gene ACT7 plays an essential role in germination and root growth. The Plant journal : for cell and molecular biology 33, 319-328.
Pubmed: Author and Title
CrossRef: Author and Title
Google Scholar: Author Only Title Only Author and Title

Granzin, J., Eckhoff, A, and Weiergraber, O.H. (2006). Crystal structure of a multi-domain immunophilin from Arabidopsis thaliana: a paradigm for regulation of plant ABC transporters. J Mol Biol 364, 799-809.
Pubmed: Author and Title
CrossRef: Author and Title
Google Scholar: Author Only Title Only Author and Title

Grebe, M. (2004). Ups and downs of tissue and planar polarity in plants. Bioessays 26, 719-729.
Pubmed: Author and Title
CrossRef: Author and Title
Google Scholar: Author Only Title Only Author and Title

Hemenway, C.S., and Heitman, J. (1996). Immunosuppressant target protein FKBP12 is required for P-glycoprotein function in yeast. The Journal of biological chemistry 271, 18527-18534.
Pubmed: Author and Title
CrossRef: Author and Title
Google Scholar: Author Only Title Only Author and Title

Henrichs, S., Wang, B., Fukao, Y., Zhu, J., Charrier, L., Bailly, A, Oehring, S.C., Linnert, M., Weiwad, M., Endler, A, Nanni, P., Pollmann, S., Mancuso, S., Schulz, A, and Geisler, M. (2012). Regulation of ABCB1/PGP1-catalysed auxin transport by linker phosphorylation. The EMBO journal 31, 2965-2980.
Pubmed: Author and Title
CrossRef: Author and Title
Google Scholar: Author Only Title Only Author and Title

Henty, J.L., Bledsoe, S.W., Khurana, P., Meagher, R.B., Day, B., Blanchoin, L., and Staiger, C.J. (2011). Arabidopsis actin depolymerizing factor4 modulates the stochastic dynamic behavior of actin filaments in the cortical array of epidermal cells. The Plant cell 23, 3711-3726.
Pubmed: Author and Title
CrossRef: Author and Title
Google Scholar: Author Only Title Only Author and Title

Henty-Ridilla, J.L., Li, J., Blanchoin, L., and Staiger, C.J. (2013). Actin dynamics in the cortical array of plant cells. Current opinion in plant biology 16, 678-687.
Pubmed: Author and Title
CrossRef: Author and Title
Google Scholar: Author Only Title Only Author and Title

Higaki, T., Kutsuna, N., Sano, T., Kondo, N., and Hasezawa, S. (2010). Quantification and cluster analysis of actin cytoskeletal structures in plant cells: role of actin bundling in stomatal movement during diurnal cycles in Arabidopsis guard cells. The Plant journal : for cell and molecular biology 61, 156-165.
Pubmed: Author and Title
CrossRef: Author and Title
Google Scholar: Author Only Title Only Author and Title

Hoffmann, C., Moreau, F., Moes, M., Luthold, C., Dieterle, M., Goretti, E., Neumann, K., Steinmetz, A, and Thomas, C. (2014a). Human muscle LIM protein dimerizes along the actin cytoskeleton and cross-links actin filaments. Molecular and cellular biology 34, 3053-3065.
Pubmed: Author and Title
CrossRef: Author and Title
Google Scholar: Author Only Title Only Author and Title

Hoffmann, C., Moes, D., Dieterle, M., Neumann, K., Moreau, F., Tavares Furtado, A, Dumas, D., Steinmetz, A, and Thomas, C. (2014b). Live cell imaging reveals actin-cytoskeleton-induced self-association of the actin-bundling protein WLIM1. Journal of cell science 127, 583-598.
Pubmed: Author and Title
CrossRef: Author and Title
Google Scholar: Author Only Title Only Author and Title

Holweg, C., and Nick, P. (2004). Arabidopsis myosin XI mutant is defective in organelle movement and polar auxin transport. Proceedings of the National Academy of Sciences of the United States of America 101, 10488-10493.
Pubmed: Author and Title
CrossRef: Author and Title
Google Scholar: Author Only Title Only Author and Title

Holweg, C., Susslin, C., and Nick, P. (2004). Capturing in vivo dynamics of the actin cytoskeleton stimulated by auxin or light. Plant & cell physiology 45, 855-863.
Pubmed: Author and Title
CrossRef: Author and Title
Google Scholar: Author Only Title Only Author and Title

Jacobs, M., and Rubery, P.H. (1988). Naturally-Occurring Auxin Transport Regulators. Science 241, 346-349.

Pubmed: Author and Title
CrossRef: Author and Title
Google Scholar: Author Only Title Only Author and Title

Kamphausen, T., Fanghanel, J., Neumann, D., Schulz, B., and Rahfeld, J.U. (2002). Characterization of Arabidopsis thaliana AtFKBP42 that is membrane-bound and interacts with Hsp90. The Plant journal : for cell and molecular biology 32, 263-276.
Pubmed: Author and Title
CrossRef: Author and Title
Google Scholar: Author Only Title Only Author and Title

Kandasamy, M.K., McKinney, E.C., and Meagher, R.B. (2009). A single vegetative actin isovariant overexpressed under the control of multiple regulatory sequences is sufficient for normal Arabidopsis development. The Plant cell 21, 701-718.
Pubmed: Author and Title
CrossRef: Author and Title
Google Scholar: Author Only Title Only Author and Title

Kandasamy, M.K., Gilliland, L.U., McKinney, E.C., and Meagher, R.B. (2001). One plant actin isovariant, ACT7, is induced by auxin and required for normal callus formation. The Plant cell 13, 1541-1554.
Pubmed: Author and Title
CrossRef: Author and Title
Google Scholar: Author Only Title Only Author and Title

Kania, U., Fendrych, M., and Friml, J. (2014). Polar delivery in plants; commonalities and differences to animal epithelial cells. Open biology 4, 140017.
Pubmed: Author and Title
CrossRef: Author and Title
Google Scholar: Author Only Title Only Author and Title

Kiefer, C.S., Claes, A.R., Nzayisenga, J.C., Pietra, S., Stanislas, T., Huser, A, Ikeda, Y., and Grebe, M. (2015). Arabidopsis AIP1-2 restricted by WER-mediated patterning modulates planar polarity. Development 142, 151-161.
Pubmed: Author and Title
CrossRef: Author and Title
Google Scholar: Author Only Title Only Author and Title

Kim, J.Y., Henrichs, S., Bailly, A, Vincenzetti, V., Sovero, V., Mancuso, S., Pollmann, S., Kim, D., Geisler, M., and Nam, H.G. (2010). Identification of an ABCB/P-glycoprotein-specific inhibitor of auxin transport by chemical genomics. The Journal of biological chemistry 285, 23309-23317.
Pubmed: Author and Title
CrossRef: Author and Title
Google Scholar: Author Only Title Only Author and Title

Kleine-Vehn, J., and Friml, J. (2008). Polar targeting and endocytic recycling in auxin-dependent plant development. Annual review of cell and developmental biology 24, 447-473.
Pubmed: Author and Title
CrossRef: Author and Title
Google Scholar: Author Only Title Only Author and Title

Kleine-Vehn, J., Dhonukshe, P., Swarup, R., Bennett, M., and Friml, J. (2006). Subcellular trafficking of the Arabidopsis auxin influx carrier AUX1 uses a novel pathway distinct from PIN1. The Plant cell 18, 3171-3181.
Pubmed: Author and Title
CrossRef: Author and Title
Google Scholar: Author Only Title Only Author and Title

Kubes, M., Yang, H., Richter, G.L., Cheng, Y., Mlodzinska, E., Wang, X., Blakeslee, J.J., Carraro, N., Petrasek, J., Zazimalova, E., Hoyerova, K., Peer, W.A., and Murphy, A.S. (2012). The Arabidopsis concentration-dependent influx/efflux transporter ABCB4 regulates cellular auxin levels in the root epidermis. The Plant journal : for cell and molecular biology 69, 640-654.
Pubmed: Author and Title
CrossRef: Author and Title
Google Scholar: Author Only Title Only Author and Title

Lanza, M., Garcia-Ponce, B., Castrillo, G., Catarecha, P., Sauer, M., Rodriguez-Serrano, M., Paez-Garcia, A, Sanchez-Bermejo, E., T, C.M., Leo del Puerto, Y., Sandalio, L.M., Paz-Ares, J., and Leyva, A. (2012). Role of actin cytoskeleton in brassinosteroid signaling and in its integration with the auxin response in plants. Developmental cell 22, 1275-1285.
Pubmed: Author and Title
CrossRef: Author and Title
Google Scholar: Author Only Title Only Author and Title

Li, G., Liang, W., Zhang, X., Ren, H., Hu, J., Bennett, M.J., and Zhang, D. (2014). Rice actin-binding protein RMD is a key link in the auxin-actin regulatory loop that controls cell growth. Proceedings of the National Academy of Sciences of the United States of America 111, 10377-10382.
Pubmed: Author and Title
CrossRef: Author and Title
Google Scholar: Author Only Title Only Author and Title

Luschnig, C. (2001). Auxin transport: why plants like to think BIG. Current biology : CB 11, R831-833.
Pubmed: Author and Title
CrossRef: Author and Title
Google Scholar: Author Only Title Only Author and Title

Luschnig, C. (2002). Auxin transport: ABC proteins join the club. Trends in plant science 7, 329-332.

Pubmed: Author and Title
CrossRef: Author and Title
Google Scholar: Author Only Title Only Author and Title

Mancuso, S., Marras, A.M., Magnus, V., and Baluska, F. (2005). Noninvasive and continuous recordings of auxin fluxes in intact root apex with a carbon nanotube-modified and self-referencing microelectrode. Anal Biochem 341, 344-351.
Pubmed: Author and Title
CrossRef: Author and Title
Google Scholar: Author Only Title Only Author and Title

Masucci, J.D., and Schiefelbein, J.W. (1994). The rhd6 Mutation of Arabidopsis thaliana Alters Root-Hair Initiation through an Auxin- and Ethylene-Associated Process. Plant physiology 106, 1335-1346.
Pubmed: Author and Title
CrossRef: Author and Title
Google Scholar: Author Only Title Only Author and Title

Muday, G.K. (2000). Maintenance of asymmetric cellular localization of an auxin transport protein through interaction with the actin cytoskeleton. Journal of plant growth regulation 19, 385-396.
Pubmed: Author and Title
CrossRef: Author and Title
Google Scholar: Author Only Title Only Author and Title

Muday, G.K., and Murphy, A.S. (2002). An emerging model of auxin transport regulation. The Plant cell 14, 293-299.
Pubmed: Author and Title
CrossRef: Author and Title
Google Scholar: Author Only Title Only Author and Title

Murphy, A.S., Hoogner, K.R., Peer, W.A., and Taiz, L. (2002). Identification, purification, and molecular cloning of N-1-naphthylphthalmic acid-binding plasma membrane-associated aminopeptidases from Arabidopsis. Plant physiology 128, 935-950.
Pubmed: Author and Title
CrossRef: Author and Title
Google Scholar: Author Only Title Only Author and Title

Mussar, K.J., Kandasamy, M.K., McKinney, E.C., and Meagher, R.B. (2015). Arabidopsis plants deficient in constitutive class profilins reveal independent and quantitative genetic effects. BMC plant biology 15, 177.
Pubmed: Author and Title
CrossRef: Author and Title
Google Scholar: Author Only Title Only Author and Title

Nagashima, A., Suzuki, G., Uehara, Y., Saji, K., Furukawa, T., Koshiba, T., Sekimoto, M., Fujioka, S., Kuroha, T., Kojima, M., Sakakibara, H., Fujisawa, N., Okada, K., and Sakai, T. (2008). Phytochromes and cryptochromes regulate the differential growth of Arabidopsis hypocotyls in both a PGP19-dependent and a PGP19-independent manner. The Plant journal : for cell and molecular biology 53, 516-529.
Pubmed: Author and Title
CrossRef: Author and Title
Google Scholar: Author Only Title Only Author and Title

Nick, P., Han, M.J., and An, G. (2009). Auxin stimulates its own transport by shaping actin filaments. Plant physiology 151, 155-167.
Pubmed: Author and Title
CrossRef: Author and Title
Google Scholar: Author Only Title Only Author and Title

Okada, K., Ueda, J., Komaki, M.K., Bell, C.J., and Shimura, Y. (1991). Requirement of the Auxin Polar Transport System in Early Stages of Arabidopsis Floral Bud Formation. The Plant cell 3, 677-684.
Pubmed: Author and Title
CrossRef: Author and Title
Google Scholar: Author Only Title Only Author and Title

Ottenschlager, I., Wolff, P., Wolverton, C., Bhalerao, R.P., Sandberg, G., Ishikawa, H., Evans, M., and Palme, K. (2003). Gravity-regulated differential auxin transport from columella to lateral root cap cells. Proceedings of the National Academy of Sciences of the United States of America 100, 2987-2991.
Pubmed: Author and Title
CrossRef: Author and Title
Google Scholar: Author Only Title Only Author and Title

Paciorek, T., Zazimalova, E., Ruthardt, N., Petrasek, J., Stierhof, Y.D., Kleine-Vehn, J., Morris, D.A., Emans, N., Jurgens, G., Geldner, N., and Friml, J. (2005). Auxin inhibits endocytosis and promotes its own efflux from cells. Nature 435, 1251-1256.
Pubmed: Author and Title
CrossRef: Author and Title
Google Scholar: Author Only Title Only Author and Title

Papuga, J., Hoffmann, C., Dieterle, M., Moes, D., Moreau, F., Tholl, S., Steinmetz, A., and Thomas, C. (2010). Arabidopsis LIM proteins: a family of actin bundlers with distinct expression patterns and modes of regulation. The Plant cell 22, 3034-3052.
Pubmed: Author and Title
CrossRef: Author and Title
Google Scholar: Author Only Title Only Author and Title

Peer, W.A., and Murphy, A.S. (2007). Flavonoids and auxin transport: modulators or regulators? Trends in plant science 12, 556-563.
Pubmed: Author and Title
CrossRef: Author and Title
Google Scholar: Author Only Title Only Author and Title

Peer, W.A., Hosein, F.N., Bandyopadhyay, A, Makam, S.N., Otegui, M.S., Lee, G.J., Blakeslee, J.J., Cheng, Y., Titapiwatanakun, B., Yakubov, B., Bangari, B., and Murphy, A.S. (2009). Mutation of the membrane-associated M1 protease APM1 results in distinct embryonic and seedling developmental defects in Arabidopsis. The Plant cell 21, 1693-1721.
  Pubmed: Author and Title
  CrossRef: Author and Title
  Google Scholar: Author Only Title Only Author and Title

Petrasek, J., Cerna, A, Schwarzerova, K., Elckner, M., Morris, D.A., and Zazimalova, E. (2003). Do phytotropins inhibit auxin efflux by impairing vesicle traffic? Plant physiology 131, 254-263.
  Pubmed: Author and Title
  CrossRef: Author and Title
  Google Scholar: Author Only Title Only Author and Title

Petrasek, J., Mravec, J., Bouchard, R., Blakeslee, J.J., Abas, M., Seifertova, D., Wisniewska, J., Tadele, Z, Kubes, M., Covanova, M., Dhonukshe, P., Skupa, P., Benkova, E., Perry, L., Krecek, P., Lee, O.R., Fink, G.R., Geisler, M., Murphy, A.S., Luschnig, C., Zazimalova, E., and Friml, J. (2006). PIN proteins perform a rate-limiting function in cellular auxin efflux. Science 312, 914-918.
  Pubmed: Author and Title
  CrossRef: Author and Title
  Google Scholar: Author Only Title Only Author and Title

Rahman, A, Bannigan, A, Sulaman, W., Pechter, P., Blancaflor, E.B., and Baskin, T.I. (2007). Auxin, actin and growth of the Arabidopsis thaliana primary root. The Plant journal : for cell and molecular biology 50, 514-528.
  Pubmed: Author and Title
  CrossRef: Author and Title
  Google Scholar: Author Only Title Only Author and Title

Rojas-Pierce, M., Titapiwatanakun, B., Sohn, E.J., Fang, F., Larive, C.K., Blakeslee, J., Cheng, Y., Cutler, S.R., Peer, W.A., Murphy, A.S., and Raikhel, N.V. (2007). Arabidopsis P-glycoprotein19 participates in the inhibition of gravitropism by gravacin. Chem Biol 14, 1366-1376.
  Pubmed: Author and Title
  CrossRef: Author and Title
  Google Scholar: Author Only Title Only Author and Title

Scheidt, H.A, Vogel, A, Eckhoff, A, Koenig, B.W., and Huster, D. (2006). Solid-state NMR characterization of the putative membrane anchor of TWD1 from Arabidopsis thaliana. Eur Biophys J.
  Pubmed: Author and Title
  CrossRef: Author and Title
  Google Scholar: Author Only Title Only Author and Title

Schenck, D., Christian, M., Jones, A, and Luthen, H. (2010). Rapid auxin-induced cell expansion and gene expression: a four-decade-old question revisited. Plant physiology 152, 1183-1185.
  Pubmed: Author and Title
  CrossRef: Author and Title
  Google Scholar: Author Only Title Only Author and Title

Seeliger, D., and de Groot, B.L. (2010). Ligand docking and binding site analysis with PyMOL and Autodock/Vina. Journal of computer-aided molecular design 24, 417-422.
  Pubmed: Author and Title
  CrossRef: Author and Title
  Google Scholar: Author Only Title Only Author and Title

Sheahan, M.B., Staiger, C.J., Rose, R.J., and McCurdy, D.W. (2004). A green fluorescent protein fusion to actin-binding domain 2 of Arabidopsis fimbrin highlights new features of a dynamic actin cytoskeleton in live plant cells. Plant physiology 136, 3968-3978.
  Pubmed: Author and Title
  CrossRef: Author and Title
  Google Scholar: Author Only Title Only Author and Title

Staiger, C.J., Sheahan, M.B., Khurana, P., Wang, X., McCurdy, D.W., and Blanchoin, L. (2009). Actin filament dynamics are dominated by rapid growth and severing activity in the Arabidopsis cortical array. The Journal of cell biology 184, 269-280.
  Pubmed: Author and Title
  CrossRef: Author and Title
  Google Scholar: Author Only Title Only Author and Title

Szymanski, W.G., Zauber, H., Erban, A, Gorka, M., Wu, X.N., and Schulze, W.X. (2015). Cytoskeletal Components Define Protein Location to Membrane Microdomains. Molecular & cellular proteomics : MCP 14, 2493-2509.
  Pubmed: Author and Title
  CrossRef: Author and Title
  Google Scholar: Author Only Title Only Author and Title

Thomas, C. (2012). Bundling actin filaments from membranes: some novel players. Frontiers in plant science 3, 188.
  Pubmed: Author and Title
  CrossRef: Author and Title
  Google Scholar: Author Only Title Only Author and Title

Titapiwatanakun, B., Blakeslee, J.J., Bandyopadhyay, A, Yang, H., Mravec, J., Sauer, M., Cheng, Y., Adamec, J., Nagashima, A, Geisler, M., Sakai, T., Friml, J., Peer, W.A., and Murphy, A.S. (2009). ABCB19/PGP19 stabilises PIN1 in membrane microdomains in Arabidopsis. The Plant journal : for cell and molecular biology 57, 27-44.
  Pubmed: Author and Title
  CrossRef: Author and Title

Google Scholar: Author Only Title Only Author and Title

van der Honing, H.S., Kieft, H., Emons, A.M., and Ketelaar, T. (2012). Arabidopsis VILLIN2 and VILLIN3 are required for the generation of thick actin filament bundles and for directional organ growth. Plant physiology 158, 1426-1438.
Pubmed: Author and Title
CrossRef: Author and Title
Google Scholar: Author Only Title Only Author and Title

Vanneste, S., and Friml, J. (2009). Auxin: a trigger for change in plant development. Cell 136, 1005-1016.
Pubmed: Author and Title
CrossRef: Author and Title
Google Scholar: Author Only Title Only Author and Title

Wang, B., Bailly, A, Zwiewka, M., Henrichs, S., Azzarello, E., Mancuso, S., Maeshima, M., Friml, J., Schulz, A, and Geisler, M. (2013). Arabidopsis TWISTED DWARF1 functionally interacts with auxin exporter ABCB1 on the root plasma membrane. The Plant cell 25, 202-214.
Pubmed: Author and Title
CrossRef: Author and Title
Google Scholar: Author Only Title Only Author and Title

Weiergraber, O.H., Eckhoff, A., and Granzin, J. (2006). Crystal structure of a plant immunophilin domain involved in regulation of MDR-type ABC transporters. FEBS letters 580, 251-255.
Pubmed: Author and Title
CrossRef: Author and Title
Google Scholar: Author Only Title Only Author and Title

Wu, G., Otegui, M.S., and Spalding, E.P. (2010). The ER-localized TWD1 immunophilin is necessary for localization of multidrug resistance-like proteins required for polar auxin transport in Arabidopsis roots. The Plant cell 22, 3295-3304.
Pubmed: Author and Title
CrossRef: Author and Title
Google Scholar: Author Only Title Only Author and Title

Wu, S., Xie, Y., Zhang, J., Ren, Y., Zhang, X., Wang, J., Guo, X., Wu, F., Sheng, P., Wang, J., Wu, C., Wang, H., Huang, S., and Wan, J. (2015). VLN2 Regulates Plant Architecture by Affecting Microfilament Dynamics and Polar Auxin Transport in Rice. The Plant cell 27, 2829-2845.
Pubmed: Author and Title
CrossRef: Author and Title
Google Scholar: Author Only Title Only Author and Title

Yu, J.H., Crevenna, A.H., Bettenbuhl, M., Freisinger, T., and Wedlich-Soldner, R. (2011). Cortical actin dynamics driven by formins and myosin V. Journal of cell science 124, 1533-1541.
Pubmed: Author and Title
CrossRef: Author and Title
Google Scholar: Author Only Title Only Author and Title

Zadnikova, P., Petrasek, J., Marhavy, P., Raz, V., Vandenbussche, F., Ding, Z, Schwarzerova, K., Morita, M.T., Tasaka, M., Hejatko, J., Van Der Straeten, D., Friml, J., and Benkova, E. (2010). Role of PIN-mediated auxin efflux in apical hook development of Arabidopsis thaliana. Development 137, 607-617.
Pubmed: Author and Title
CrossRef: Author and Title
Google Scholar: Author Only Title Only Author and Title

Zhu, J., and Geisler, M. (2015b). Keeping it all together: auxin-actin crosstalk in plant development. Journal of experimental botany 66, 4983-4998.
Pubmed: Author and Title
CrossRef: Author and Title
Google Scholar: Author Only Title Only Author and Title

TWISTED DWARF1 mediates the action of auxin transport inhibitors on actin cytoskeleton dynamics.

Jinsheng Zhu, Aur?lien Bailly, Marta Zwiewka, Valpuri Sovero, Martin di Donato, Pei Ge, Jacqueline Oehri, Bibek Aryal, Pengchao Hao, Miriam Linnert, Noelia Burgardt, Christian Lücke, Matthias Weiwad, Max Michel, Oliver H Weiergräber, Stephan Pollmann, Elisa Azzarello, Stefano Mancuso, Noel Ferro, Yoichiro Fukao, Celine Hoffmann, Roland Wedlich-Söldner, Jiri Friml, Clement Thomas and Markus Geisler

This information is current as of September 16, 2016

Supplemental Data	**http://www.plantcell.org/content/suppl/2016/04/06/tpc.15.00726.DC1.html**
Permissions	https://www.copyright.com/ccc/openurl.do?sid=pd_hw1532298X&issn=1532298X&WT.mc_id=pd_hw1532298X
eTOCs	Sign up for eTOCs at: http://www.plantcell.org/cgi/alerts/ctmain
CiteTrack Alerts	Sign up for CiteTrack Alerts at: http://www.plantcell.org/cgi/alerts/ctmain
Subscription Information	Subscription Information for *The Plant Cell* and *Plant Physiology* is available at: http://www.aspb.org/publications/subscriptions.cfm